Color neutral two-flavor superconducting phase of cold and dense quark matter in the presence of constant magnetic fields

Sh. Fayazbakhsh* and N. Sadooghi†

Department of Physics, Sharif University of Technology, P.O. Box 11155-9161, Tehran-Iran

(Received 26 May 2010; published 9 August 2010)

The color neutral two-flavor superconducting phase of cold and dense quark matter is studied in the presence of constant magnetic fields and at moderate baryon densities. In the first part of the paper, a two-flavor effective Nambu–Jona-Lasinio model consisting of a chiral symmetry breaking (χSB) mass gap σ_B, a color superconducting (CSC) mass gap Δ_B and a color chemical potential μ_8 is introduced in the presence of a rotated $U(1)$ magnetic field $\tilde{\mathbf{B}}$. To study the phenomenon of magnetic catalysis in the presence of strong magnetic fields, the gap equations corresponding to σ_B and Δ_B, as well as μ_8 are solved in the lowest Landau level approximation. In the second part of the paper, a detailed numerical analysis is performed to explore the effect of any arbitrary magnetic field on the above mass gaps and the color chemical potential. The structure of the χSB and CSC phases is also presented in the μ_c-$\tilde{e}B$ plane, and the effect of μ_8 on the phase structure of the model is explored. As it turns out, whereas the transition from the χSB to CSC phase is of first order, nonvanishing μ_8 affects essentially the second order phase transition from CSC to the normal phase.

DOI: 10.1103/PhysRevD.82.045010 PACS numbers: 12.38.−t, 11.30.Qc, 12.38.Aw, 12.39.−x

I. INTRODUCTION

Dense baryonic matter at low temperature and asymptotically large chemical potential is known to be a color superconductor [1]. This can be shown in the framework of perturbative quantum chromodynamics (pQCD). To explore the color superconducting phase at moderate chemical potential, however, it is necessary to use effective models, such as the well-known Nambu–Jona-Lasinio (NJL) model with four-fermion interaction [2]. Using an appropriate NJL-type model, one can show that at baryon densities $\mu_c \simeq 350$ MeV, i.e. only several times larger than the density of nuclear matter, the two-flavor-color superconducting (2SC) phase might be present [3,4] (see [5] for recent reviews on color superconductivity in dense quark matter). Different astrophysical processes might therefore be influenced by the color superconductivity that is supposed to exist inside the compact stars. In [6], the competition between the chiral symmetry breaking and the color symmetry breaking condensates is investigated in the framework of a two-flavor color neutral NJL-type model, including meson and diquark condensates, σ_0 and Δ_0. Imposing the color neutrality condition, it is found that in the 2SC phase at $\mu > \mu_c = 342$ MeV, the color chemical potential μ_8 acquires rather small values of about 10 MeV.[1] Here, μ_c is the critical chemical potential. The diquark mass gap is numerically computed to be $\Delta_0 \simeq 100$ MeV. It is also shown that the appearance of a coexistence regime (mixed phase) depends directly on the relative strength of the meson and diquark coupling constants G_S and G_D. This is also indicated in [8–10], where it is stated that neglecting the quark masses and choosing $G_D < G_S$, no mixed phase appears at $\mu > \mu_c$. The χSB and color superconducting (CSC) phases can therefore be studied separately under these conditions.

In the present paper, we study the mesons and diquarks in the color neutral 2SC phase of cold and dense quark matter in the presence of constant magnetic fields. The aim is to study the effect of the magnetic field on the formation of chiral as well as diquark condensates, the dependence of mass gaps on the chemical potential μ and the external magnetic field, the phase diagram μ vs B, and the effect of nonvanishing color chemical potential on the type of phase transitions for different μ and B at zero temperature T.[2]

The study of quark matter in the presence of constant magnetic field is relevant for the astrophysics of compact stars: Strong magnetic fields exist on the surface of compact stars. For neutron stars the magnetic fields $B \lesssim 10^{12}$ Gauß, whereas for magnetars, they can be as large as $B \simeq 10^{16}$ Gauß [12]. In the interiors of compact stars, the magnetic field can be even several orders of magnitude larger [13]. On the other hand, it is believed that the superdense interior of compact stars may be composed of electric and color neutral quark matter in the color superconducting phase. To test the predictions of astrophysical signatures of color superconductivity, a better understanding of the rôle of magnetic fields on the CSC phase is important. The study of superconducting phase in the presence of external magnetic fields is also relevant for

*fayyazbaksh@physics.sharif.ir
†sadooghi@physics.sharif.ir

[1]The underlying physics of color charge neutrality is discussed in [7].

[2]The effect of finite temperature will be presented elsewhere [11].

the physics of heavy ion collisions: According to [14,15], in off-central collisions, heavy ions possess a very large angular momentum and very strong magnetic fields can be created. In [16], it is shown that the magnetic field presently created at RHIC is at most $eB \simeq 1.3m_\pi^2 \sim 4.3 \times 10^{18}$ Gauß, and the estimated value of the magnetic field strength for the LHC energy amounts to $15m_\pi^2 \sim 5 \times 10^{19}$ Gauß.[3] Recently, the question of accessibility of the 2SC phase in the future heavy ion collision experiments is investigated in [17]. Here, the authors do not consider the effect of the before mentioned magnetic fields. It would be therefore important to study the effect of external magnetic fields on the formation of 2SC diquark condensates, as well as the corresponding phase structure in the presence of external magnetic fields. As for the results presented in this paper, they may be relevant only for the physics of the heavy ion collisions, because in contrary to the electric and color neutrality requirement of the superdense core of the compact stars, only the color neutrality condition is considered in this paper.

The effect of constant magnetic field on the formation of diquark condensates has been investigated by several authors. In [18,19], it is shown that there is a linear combination of photon and a gluon that remains massless. The resulting ''rotated'' external magnetic field can therefore penetrate the color superconducting region without being affected by the Meissner effect. This has consequences for the structure of compact star cores. In [20,21], the formation of magnetic color-flavor locked (MCFL) phase, as well as the transition to the paramagnetic-CFL (PCFL) phase are studied. In [22,23], it is shown that for small magnetic fields, the CFL mass gap as well as the corresponding magnetization exhibit small oscillations, the van Alfven–de Haas (vAdH) oscillations. This effect, which is well known from condensed matter physics, is predicted by Landau and observed experimentally by van Alfven and de Haas (see [24] for an investigation of this effect in cold dense quark matter in a homogeneous magnetic field). The transport properties of 2SC phase is investigated recently in [25].

Recently, in [26], the formation of chiral and diquark condensates as well as their competition in the 2SC phase at zero temperature and moderate densities are studied using the same NJL-type model as in the present paper. It is shown that for vanishing magnetic field, a mixed broken phase can be found where both chiral and superconducting gaps are nonzero. For $\tilde{e}B = 0.05$ GeV^2 (corresponding to $B \simeq 8.5 \times 10^{18}$ Gauß) and moderate diquark-to-chiral coupling ratios G_D/G_S, the chiral and superconducting transitions become weaker. For large G_D/G_S, strong magnetic fields disrupt the mixed broken phase region and a first order phase transition is found between the χSB and the CSC phase for $\tilde{e}B = 0.05$ GeV^2. In contrast to [26], our results include a detailed analytical and numerical survey on the effect of external magnetic field and color chemical potential on cold and dense as well as color neutral quark matter in the presence of external magnetic fields.

The organization of this paper is as follows: In Sec. II, starting from an extended Lagrangian density of a gauged NJL model containing two flavors, and following the method presented in [18,19], we introduce the rotated magnetic field $\tilde{e}B$ and determine the Lagrangian density containing the χSB and CSC mass gaps, σ_B and Δ_B, respectively. In Sec. III, the one-loop effective action and thermodynamic potential of the model are determined at zero temperature and finite quark chemical potential. In Sec. IV, assuming very strong magnetic fields, we solve analytically the gap equations corresponding to σ_B and Δ_B, as well as the color chemical potential μ_8 in an appropriate lowest Landau level (LLL) approximation. The χSB and the CSC phases are studied, in IV A and IV B, separately. This is possible because of our specific choice of free parameters, the quark mass m_0 and the meson and diquark couplings G_S and G_D. In the χSB phase, characterized by $\sigma_B \neq 0$ and $\Delta_B = \mu_8 = 0$, the magnetic field enhances the bound state formation. This is because of the phenomenon of magnetic catalysis [27,28] studied intensively in the past few years.[4] In the CSC phase, characterized by $\sigma_B = 0$, $\Delta_B \neq 0$ and $\mu_8 \neq 0$, we determine analytically the μ and $\tilde{e}B$ dependence of Δ_B and μ_8 in the regime of LLL dominance. In Sec. V, a numerical analysis is performed to study the $\tilde{e}B$ dependence of the χSB and CSC mass gaps at $\mu = 250$ MeV (in the χSB regime) and $\mu = 460$ MeV (in the CSC regime). For small values of $\tilde{e}B$, we observe vAdH oscillations in the mass gaps as well as the corresponding magnetizations, as expected. These are also observed in [22,23] for three-flavor CFL phase at $\mu = 500$ MeV. At $\tilde{e}B \simeq 0.45$–0.5 GeV^2, the oscillations end up in a ''linear regime.'' Comparing eventually our numerical results for $\tilde{e}B \gtrsim 0.45$ GeV^2 with the analytical results arising in Sec. IV for strong magnetic fields in the LLL approximation, we conclude that this approximation is only reliable in the above linear regime. The μ-dependence of the mass gaps and the color chemical potential is also discussed for various $\tilde{e}B$. Our results for vanishing $\tilde{e}B$ coincide with the results in [6]. We also present the phase structure of χSB and CSC phases in a μ_c-$\tilde{e}B$ plane. In particular, we are interested in the effect of the color chemical potential μ_8 on the phase structure of the model. As it turns out, for $\mu_8 = 0$, a first order phase transition exists between the χSB and the CSC phase in the regime $\mu_c \simeq 350$–450 MeV and $\tilde{e}B \in [0, 0.7]$ GeV^2, whereas the transition from the CSC to the normal phase is of second order and occurs at

[3]Here, the pion mass, $m_\pi = 140$ MeV.

[4]See [29] for the application of magnetic catalysis in cosmology, [30] for its application in condensed matter physics, and [31–34] for its applications in particle physics.

$\mu_c \simeq 750$–800 MeV. For $\mu_8 \neq 0$, however, whereas the phase transition between the χSB and the CSC phase is still of first order, the second order phase transition between the CSC and the normal phase goes over into a first order phase transition between the CSC and the normal phase at $\mu_c \simeq 755$ MeV and $\tilde{e}B \simeq 0.13$ GeV^2. Note that the first order nature of the transition between the χSB and CSC phases was expected from [26], where the type of phase transition between these two phases is studied for a fixed $\tilde{e}B = 0.05$ GeV^2 and various G_D/G_S ratios. Our results confirm the findings in [26] for a wide range of $\tilde{e}B \in \{0, 0.7\}$ GeV^2 and fixed value of $G_D/G_S = 0.75$. Section VI is devoted to a summary of our results and concluding remarks.

II. TWO FLAVOR 2SC MODEL AT $T = 0$, AND $\mu, B \neq 0$

Let us start with the fermionic part of the extended Lagrangian density of a gauged NJL model[5]

$$\begin{aligned}\mathcal{L}_f = {} & \bar{\psi}(x)[i\gamma^\mu(\partial_\mu - ieQA_\mu - igT^8G^8_\mu) - m_0 + \hat{\mu}\gamma^0]\psi(x) \\ & + G_S[(\bar{\psi}(x)\psi(x))^2 + (\bar{\psi}(x)i\gamma_5\vec{\tau}\psi(x))^2] \\ & + G_D[(i\bar{\psi}^C(x)\epsilon_f\epsilon^3_c\gamma_5\psi(x))(i\bar{\psi}(x)\varepsilon_f\epsilon^3_c\gamma_5\psi^C(x))].\end{aligned} \tag{2.1}$$

Here, $\psi^C = C\bar{\psi}^T$ and $\bar{\psi}^C = \psi^T C$ are charge-conjugate spinors, and $C = i\gamma^2\gamma^0$ is charge-conjugation matrix, $\vec{\tau} = (\tau_1, \tau_2, \tau_3)$ are Pauli matrices. Moreover, $(\epsilon^3_c)^{ab} \equiv (\epsilon_c)^{ab3}$ and $(\varepsilon_f)_{ij}$ are antisymmetric matrices in color and flavor spaces, respectively. For a theory with two quark flavors, $i, j = (1, 2) = (u, d)$, and three color degrees of freedom $a, b = (1, 2, 3) = (r, g, b)$. We assume that both quarks have the same (bare) mass $m_u = m_d \equiv m_0$.[6] Further, $\hat{\mu}$ is defined by $\hat{\mu} \equiv \mu + \sqrt{3}\mu_8\lambda_8$, where μ is the quark chemical potential and is responsible for the nonzero baryonic density of quark matter, and μ_8 is inserted by hand to impose the color neutrality after the process of dynamical color symmetry breaking. Here, $T^8 = \frac{\lambda_8}{2}$ with $\lambda_8 = \frac{1}{\sqrt{3}}\,\mathrm{diag}(1, 1, -2)$ the 8th Gell-Mann λ-matrix. The scalar and diquark couplings are denoted by G_S and G_D, respectively. Furthermore, $Q = Q_f \otimes \mathbf{1}_c$ with $Q_f \equiv \mathrm{diag}(2/3, -1/3)$ is the fermionic charge matrix coupled to $U(1)$ gauge field A_μ. The same setup without the coupling to A_μ and G^8_μ is also used in [6]. To determine the effective action of the above model, we introduce first the bosonized Lagrangian density

$$\begin{aligned}\mathcal{L}_f = {} & \bar{\psi}(x)[i\gamma^\mu(\partial_\mu - ieQA_\mu - igT^8G^8_\mu) + \hat{\mu}\gamma^0]\psi(x) \\ & - \bar{\psi}(x)(m + i\gamma^5\vec{\tau}\cdot\vec{\pi})\psi(x) \\ & - \frac{1}{2}\Delta^{*3}(i\bar{\psi}^C(x)\varepsilon_f\epsilon^3_c\gamma_5\psi(x)) \\ & - \frac{1}{2}\Delta^3(i\bar{\psi}(x)\varepsilon_f\epsilon^3_c\gamma_5\psi^C(x)) - \frac{\sigma^2 + \vec{\pi}^2}{4G_S} - \frac{\Delta^3\Delta^{*3}}{4G_D},\end{aligned} \tag{2.2}$$

with $m \equiv m_0 + \sigma$, that includes the auxiliary mesonic fields

$$\sigma = -2G_S(\bar{\psi}\psi), \qquad \vec{\pi} = -2G_S(\bar{\psi}i\gamma^5\vec{\tau}\psi), \tag{2.3}$$

and diquarks

$$\begin{aligned}\Delta^3 &= -2G_D(i\bar{\psi}^C\varepsilon_f\epsilon^3_c\gamma_5\psi), \\ \Delta^{*3} &= -2G_D(i\bar{\psi}\varepsilon_f\epsilon^3_c\gamma_5\psi^C).\end{aligned} \tag{2.4}$$

From now on, we will skip the superscript "3" for Δ and Δ^*. Using an appropriate mean field approximation, the effective potential of this model can be determined as a function of the condensates $\langle\sigma\rangle$, $\langle\vec{\pi}\rangle$,$\langle\Delta\rangle$ and $\langle\Delta^*\rangle$. For simplicity we set $\langle\vec{\pi}\rangle = \vec{0}$. It is the purpose of this paper to study the effect of a constant background $U(1)$ magnetic field on the formation of these condensates. To do this, we have, principally, to replace A_μ by a classical A^{ext}_μ and a dynamical part a_μ and then integrate out the dynamical gauge field a_μ and G^8_μ. However, it turns out that for nonvanishing (Δ, Δ^*), both gauge fields A_μ and G^8_μ are massive and underlie the Meissner effect.[7] They are therefore inappropriate to be taken as external fields. But, as it is shown in [18,19], there is indeed a linear combination of A_μ and G^8_μ, that leads to a massless rotated $U(1)$ field, $\tilde{A}_\mu = A_\mu\cos\theta - G^8_\mu\sin\theta$, and a massive rotated $SU(3)$ field, $\tilde{G}^8_\mu = A_\mu\sin\theta + G^8_\mu\cos\theta$. According to [19], the angle θ can be determined from

$$\cos\theta \equiv -\frac{\sqrt{3}g}{\sqrt{3g^2 + e^2}}, \quad \text{and} \quad \sin\theta \equiv -\frac{e}{\sqrt{3g^2 + e^2}}. \tag{2.5}$$

To rotate the fields, one uses the identity

$$eQA_\mu + gT^8G^8_\mu \equiv \tilde{e}\,\tilde{Q}\,\tilde{A}_\mu + \tilde{g}\,\tilde{T}\,\tilde{G}^8_\mu, \tag{2.6}$$

and insert the combination $\mathcal{O}\mathcal{O}^T = 1$ on the right-hand side (r.h.s.) of this identity. Here, $\mathcal{O}$ is an appropriate rotation matrix including sine and cosine of θ. The identity (2.6) not only determines the new rotated fields as a linear combination of the original nonrotated ones, it also fixes the relation between the rotated and nonrotated couplings

[5]The gauge kinetic term will be added to this Lagrangian in the last step.

[6]In Secs. IV and V, the bare mass, m_0, will be chosen to be zero.

[7]As it turns out σ is invariant under $U_V(1)$ and $SU_V(3)$ groups. Thus $Q\langle\sigma\rangle = T^8\langle\sigma\rangle = 0$, whereas $Q\langle\Delta\rangle \neq 0$ as well as $T^8\langle\Delta\rangle \neq 0$.

as $\tilde{e}\,\tilde{Q} = eQ\cos\theta - gT^8\sin\theta$, as well as $\tilde{g}\,\tilde{T} = eQ\sin\theta + gT^8\cos\theta$. In the rotated system, one chooses $\tilde{Q}$ so that $\tilde{Q}\langle\Delta\rangle = 0$. This leads to

$$\tilde{Q} = Q_f \otimes \mathbf{1}_c - \mathbf{1}_f \otimes \left(\frac{T^8}{\sqrt{3}}\right)_c. \tag{2.7}$$

The above relations between the rotated and nonrotated generators, (Q, T^8) and $(\tilde{Q}, \tilde{T})$, lead then to $\tilde{T}\langle\Delta\rangle \neq 0$, which then yields a nonvanishing mass for $\tilde{G}^8_\mu$. Hence, as long as the diquark condensate Δ is nonvanishing, the rotated $\tilde{G}^8_\mu$ is massive because of $\tilde{T}\langle\Delta\rangle \neq 0$. In this case, the rotated system is the true physical system. Once $\Delta = 0$ and $\sigma \neq 0$, the rotated and nonrotated systems are equivalent, because the identity $\tilde{Q}\langle\sigma\rangle = \tilde{T}\langle\sigma\rangle = 0$ holds automatically. Using (2.7) and the above relation $\tilde{e}\,\tilde{Q} = eQ\cos\theta - gT^8\sin\theta$ between the rotated $\tilde{e}\,\tilde{Q}$ and the nonrotated eQ, it turns out that $\tilde{e} \equiv e\cos\theta$, as in the electroweak standard model.[8] In the six-dimensional flavor-color representation, $(u_r, u_g, u_b, d_r, d_g, d_b)$, the rotated $\tilde{Q}$ charges of different quarks, in units of $\tilde{e}$, are presented in Table I.

Plugging (2.6) in (2.2), the resulting transformed Lagrangian density is then given by (2.2) with $eQA_\mu + gT^8G^8_\mu$ replaced by $\tilde{e}\,\tilde{Q}\,\tilde{A}_\mu + \tilde{g}\,\tilde{T}\,\tilde{G}^8_\mu$, and $\vec{\pi} = \vec{0}$ [see (2.6)], and reads

$$\begin{aligned}\mathcal{L}_f = {} & \bar{\psi}(x)[i\gamma^\mu(\partial_\mu - i\tilde{e}\,\tilde{Q}\,\tilde{A}_\mu - i\tilde{g}\,\tilde{T}\,\tilde{G}^8_\mu) + \hat{\mu}\gamma^0]\psi(x) \\ & - m\bar{\psi}(x)\psi(x) - \frac{1}{2}\Delta^*(i\bar{\psi}^C(x)\varepsilon_f\epsilon^3_c\gamma_5\psi(x)) \\ & - \frac{1}{2}\Delta(i\bar{\psi}(x)\varepsilon_f\epsilon^3_c\gamma_5\psi^C(x)) - \frac{\sigma^2}{4G_S} - \frac{|\Delta|^2}{4G_D},\end{aligned} \tag{2.8}$$

with $|\Delta|^2 \equiv \Delta\Delta^*$. To introduce the external rotated $U(1)$ magnetic field in the third direction, we replace $\tilde{A}_\mu \to \tilde{A}^{\text{ext}}_\mu + \tilde{a}_\mu$, with the external rotated electromagnetic field $\tilde{A}^{\text{ext}}_\mu$ in the Landau gauge $\tilde{A}^{\text{ext}}_\mu = (0, 0, Bx, 0)$, and integrate out the remaining dynamical rotated fields $\tilde{a}_\mu$ and $\tilde{G}^8_\mu$. We arrive therefore at the full modified bosonized Lagrangian $\tilde{\mathcal{L}} = \tilde{\mathcal{L}}_k + \tilde{\mathcal{L}}_f$, with[9]

$$\tilde{\mathcal{L}}_k \equiv -\left(\frac{\sigma^2}{4G_S} + \frac{|\Delta|^2}{4G_D} + \frac{B^2}{2}\right), \tag{2.9}$$

and

$$\begin{aligned}\tilde{\mathcal{L}}_f = {} & \bar{\psi}(x)[i\gamma^\mu(\partial_\mu - i\tilde{e}\,\tilde{Q}\,\tilde{A}^{\text{ext}}_\mu) + \hat{\mu}\gamma^0]\psi(x) \\ & - m\bar{\psi}(x)\psi(x) - \tfrac{1}{2}\Delta^*(i\bar{\psi}^C(x)\varepsilon_f\epsilon^3_c\gamma_5\psi(x)) \\ & - \tfrac{1}{2}\Delta(i\bar{\psi}(x)\varepsilon_f\epsilon^3_c\gamma_5\psi^C(x)),\end{aligned} \tag{2.10}$$

[8]In a system including mesons and diquarks, only diquarks play the role of electroweak Higgs field.

[9]Comparing to (2.8), in (2.9), we have added the kinetic term of the rotated $U(1)$ external gauge field $-\frac{1}{4}(F_{\mu\nu})^2|_{\tilde{A}_{\text{ext}}} = -\frac{B^2}{2}$.

TABLE I. $\tilde{Q}$ charges of quarks in 2SC model in the presence of rotated magnetic field $\tilde{\mathbf{B}}$ in units of $\tilde{e}$.

quarks	u_r	u_g	u_b	d_r	d_g	d_b
$\tilde{q}$	$+\frac{1}{2}$	$+\frac{1}{2}$	1	$-\frac{1}{2}$	$-\frac{1}{2}$	0

in a constant (rotated) background $U(1)$ magnetic field $\tilde{\mathbf{B}} = B\mathbf{e}_3$. In what follows, we will simplify (2.10) using the method presented in [20] and arrive at an equivalent Lagrangian, which will then be used in Sec. III to determine the effective potential of the above model in the presence of a rotated background $U(1)$ magnetic field $\tilde{\mathbf{B}}$. To do this, we introduce the rotated-charge projectors $\Omega_{\tilde{q}}$, that satisfy the eigenvalue equation $\tilde{Q}\Omega_{\tilde{q}} = \tilde{q}\Omega_{\tilde{q}}$. They are given by

$$\begin{aligned}\Omega_0 &= \text{diag}(0, 0, 0, 0, 0, 1), \\ \Omega_{+1/2} &= \text{diag}(1, 1, 0, 0, 0, 0), \\ \Omega_1 &= \text{diag}(0, 0, 1, 0, 0, 0), \\ \Omega_{-1/2} &= \text{diag}(0, 0, 0, 1, 1, 0),\end{aligned}$$

and satisfy

$$\sum_{\tilde{q}\in\{0,1,\pm(1/2)\}} \Omega_{\tilde{q}} = 1, \quad \text{and} \quad \Omega_{\tilde{q}}\Omega_{\tilde{q}'} = \delta_{\tilde{q}\tilde{q}'}. \tag{2.11}$$

Using the definition $\psi_{\tilde{q}}(x) \equiv \Omega_{\tilde{q}}\psi(x)$, the fermion field in the six-dimensional color-flavor representation can now be given by

$$\psi = \sum_{\tilde{q}\in\{0,1,\pm(1/2)\}} \psi_{\tilde{q}}. \tag{2.12}$$

Introducing, at this stage, the Nambu-Gorkov bispinor wave function

$$\Psi_{\tilde{q}} = \begin{pmatrix} \psi_{\tilde{q}} \\ \psi^C_{-\tilde{q}} \end{pmatrix},$$

the part of the Lagrangian which is bilinear in ψ, i.e. $\tilde{\mathcal{L}}_f$ from (2.10), can be brought in the following form:

$$\tilde{\mathcal{L}}_f = \frac{1}{2}\sum_{\tilde{q}\in\{0,1,\pm(1/2)\}} \bar{\Psi}_{\tilde{q}}(x)\mathcal{S}_{\tilde{q}}\Psi_{\tilde{q}}(x), \tag{2.13}$$

where $\mathcal{S}_{\tilde{q}}$ for $\tilde{q} \in \{0, 1\}$ is given by

$$\mathcal{S}_{\tilde{q}\in\{0,1\}} \equiv \begin{pmatrix} [G^+_{(\tilde{q})}]^{-1} & 0 \\ 0 & [G^-_{(\tilde{q})}]^{-1} \end{pmatrix}, \tag{2.14}$$

and for $\tilde{q} \in \{-\frac{1}{2}, +\frac{1}{2}\}$ by

$$\mathcal{S}_{\tilde{q}\in\{-(1/2),+(1/2)\}} \equiv \begin{pmatrix} [G^+_{(\tilde{q})}]^{-1} & -\kappa\Omega_{-\tilde{q}} \\ -\kappa'\Omega_{\tilde{q}} & [G^-_{(\tilde{q})}]^{-1} \end{pmatrix}. \tag{2.15}$$

Here, $[G^{\pm}_{(\tilde{q})}]^{-1} \equiv [\gamma^{\mu}(i\partial_{\mu} + \tilde{e}\,\tilde{q}\,\tilde{A}_{\mu} \pm \hat{\mu}\,\delta_{\mu 0}) - m]$, and $\kappa^{ij,ab}_{\alpha\beta} \equiv i\Delta\tau_2^{ij}\lambda_2^{ab}\gamma^5_{\alpha\beta}$ as well as $\kappa' \equiv \gamma_0\kappa^{\dagger}\gamma_0 = i\Delta^*\tau_2\lambda_2\gamma^5$. They can be read from (2.10) and the relations (2.11) as well as the definition of $\psi_{\tilde{q}} = \Omega_{\tilde{q}}\psi$. Note that (2.13) can be equivalently expressed as

$$\begin{aligned}\tilde{\mathcal{L}}_f = \frac{1}{2}\sum_{\tilde{q}\in\{0,1,\pm(1/2)\}} \{&\bar{\psi}^C_{\tilde{q}}(x)[G^-_{(-\tilde{q})}]^{-1}\psi^C_{\tilde{q}}(x) \\ &+ \bar{\psi}_{\tilde{q}}(x)[G^+_{(\tilde{q})}]^{-1}\psi_{\tilde{q}}(x) - \bar{\psi}^C_{\tilde{q}}(x)\tilde{\kappa}'_{\tilde{q}}\psi_{\tilde{q}}(x) \\ &- \bar{\psi}_{\tilde{q}}(x)\tilde{\kappa}_{\tilde{q}}\psi^C_{\tilde{q}}(x)\},\end{aligned} \tag{2.16}$$

where, $\tilde{\kappa}_{\tilde{q}}$ is defined by $\tilde{\kappa}_{\tilde{q}} \equiv \Omega_{\tilde{q}'}\kappa\Omega_{\tilde{q}}$. In (2.16), $\tilde{\kappa}_{\tilde{q}}$ is nonvanishing only for $\tilde{q}' + \tilde{q} = 0$ with $\tilde{q}' \neq \tilde{q}$. For $\tilde{q} \in \{-\frac{1}{2}, +\frac{1}{2}\}$ we have therefore

$$\begin{aligned}(\tilde{\kappa}_{\tilde{q}=-1/2})_{\rho\sigma} &= (\Omega_{1/2}\kappa\Omega_{-1/2})_{\rho\sigma} = (\kappa\Omega_{-1/2})_{\rho\sigma} \\ &= \begin{cases} +i\Delta\gamma^5 & \text{if } (\rho,\sigma) = (2,4), \\ -i\Delta\gamma^5 & \text{if } (\rho,\sigma) = (1,5), \\ 0 & \text{otherwise,}\end{cases}\end{aligned} \tag{2.17}$$

$$\begin{aligned}(\tilde{\kappa}_{\tilde{q}=+1/2})_{\rho\sigma} &= (\Omega_{-(1/2)}\kappa\Omega_{1/2})_{\rho\sigma} = (\kappa\Omega_{+1/2})_{\rho\sigma} \\ &= \begin{cases} +i\Delta\gamma^5 & \text{if } (\rho,\sigma) = (4,2), \\ -i\Delta\gamma^5 & \text{if } (\rho,\sigma) = (5,1), \\ 0 & \text{otherwise,}\end{cases}\end{aligned} \tag{2.18}$$

whereas for $\tilde{q} \in \{0, 1\}$, we have

$$\tilde{\kappa}_{ij} = (\Omega_i\kappa\Omega_j)_{\rho\sigma} = 0, \quad \text{for } i,j = 0,1 \quad \text{or} \quad i = j = \pm\tfrac{1}{2}. \tag{2.19}$$

This is in contrast to the case of three-flavor color-flavor locked (CFL) phase, studied in [20]. In that case, there exists a charge $\tilde{q} = -1$ and the combination of $(\Omega_{\mp 1}\kappa\Omega_{\pm 1})$ leads also to nonzero result.

III. ONE-LOOP EFFECTIVE ACTION AND THERMODYNAMIC POTENTIAL

In what follows, the one-loop effective action of the theory, Γ, will be determined in the mean field approximation in terms of $\sigma \equiv \langle\sigma(x)\rangle$, $\Delta \equiv \langle\Delta(x)\rangle$, and $\Delta^* \equiv \langle\Delta^*(x)\rangle$. Using the following path integral over the quark fields

$$e^{i\Gamma[\sigma,\Delta,\Delta^*]} = \int \mathcal{D}\psi\mathcal{D}\bar{\psi}\exp\left(i\int d^4x\tilde{\mathcal{L}}\right), \tag{3.1}$$

where, $\tilde{\mathcal{L}} \equiv \tilde{\mathcal{L}}_k + \tilde{\mathcal{L}}_f$, with $\tilde{\mathcal{L}}_k$ and $\tilde{\mathcal{L}}_f$ from (2.9) and (2.13), the effective action up to one-loop quantum corrections is given by

$$\Gamma[\sigma,\Delta,\Delta^*] = -\left(\frac{\sigma^2}{4G_S} + \frac{|\Delta|^2}{4G_D} + \frac{B^2}{2}\right)\mathcal{V} + \Gamma^{(1)}_{\text{eff}}[\sigma,\Delta,\Delta^*]. \tag{3.2}$$

Here, $\mathcal{V}$ is the four-dimensional space-time volume, and $\Gamma^{(1)}_{\text{eff}}$ is the one-loop contribution to the effective potential. It arises by integrating out the fermion fields and reads

$$\Gamma^{(1)}_{\text{eff}} = -\frac{i}{2}\sum_{\tilde{q}}\text{Tr}_{\{\text{NG}cfsx\}}\ln[\mathcal{S}^{-1}_{\tilde{q}}], \tag{3.3}$$

where $\mathcal{S}_{\tilde{q}}$ is defined in (2.14) and (2.15). Here, the trace "Tr" operation in (3.3) includes apart from a two-dimensional trace in the Nambu-Gorkov (NG) space, a trace over the whole phase space. It is therefore defined by a trace over the color (c), flavor (f), and spinor (s) degrees of freedom, as well as over a four-dimensional space-time coordinate (x) [6]. To compute (3.3), we have to notice that, according to Table I, the blue quarks (u_b, d_b) have $\tilde{q} = 0$, 1, whereas the green and red quarks (u_r, u_g, d_r, d_g) have $\tilde{q} = \pm\frac{1}{2}$. Thus relation (3.3) reduces to

$$\Gamma^{(1)}_{\text{eff}} = \sum_{\kappa\in\{r,g,b\}}\Gamma^{(1)/\kappa}_{\text{eff}}, \tag{3.4}$$

where the one-loop effective action of the blue (b) and red/green (r/g) are given by

$$\begin{aligned}\Gamma^{(1)/b}_{\text{eff}} &= -\frac{i}{2}\,\text{Tr}_{\{\text{NG}cfsx\}}\ln[{\mathcal{S}_0}^{-1}] \\ &\quad -\frac{i}{2}\,\text{Tr}_{\{\text{NG}cfsx\}}\ln[{\mathcal{S}_{+1}}^{-1}], \\ \sum_{\kappa\in\{r,g\}}\Gamma^{(1)/\kappa}_{\text{eff}} &= -\frac{i}{2}\,\text{Tr}_{\{\text{NG}cfsx\}}\ln[{\mathcal{S}_{+1/2}}^{-1}] \\ &\quad -\frac{i}{2}\,\text{Tr}_{\{\text{NG}cfsx\}}\ln[{\mathcal{S}_{-1/2}}^{-1}].\end{aligned} \tag{3.5}$$

To perform the trace operation in the NG space, we use

$$\begin{aligned}\det\begin{pmatrix}A & B\\ C & D\end{pmatrix} &= \det(-BC + BDB^{-1}A) \\ &= \det(-CB + CAC^{-1}D).\end{aligned} \tag{3.6}$$

Using further $\text{tr}\ln A = \ln\det A$, we arrive at

$$\begin{aligned}\det_{\{\text{NG}cfsx\}}[{\mathcal{S}_0}^{-1}] &= \det_{\{scx\}}[\{\gamma^{\alpha}(i\partial_{\alpha} + \breve{\mu}\,\delta_{\alpha 0}) - m\} \\ &\quad \times\{\gamma^{\alpha}(i\partial_{\alpha} - \breve{\mu}\,\delta_{\alpha 0}) - m\}], \\ \det_{\{\text{NG}cfsx\}}[{\mathcal{S}_{+1}}^{-1}] &= \det_{\{scx\}}[\{\gamma^{\alpha}(i\partial_{\alpha} + \tilde{e}\tilde{A}_{\alpha} + \breve{\mu}\,\delta_{\alpha 0}) - m\} \\ &\quad \times\{\gamma^{\alpha}(i\partial_{\alpha} + \tilde{e}\tilde{A}_{\alpha} - \breve{\mu}\,\delta_{\alpha 0}) - m\}], \\ \det_{\{\text{NG}cfsx\}}[{\mathcal{S}_{\pm 1/2}}^{-1}] &= \det_{\{scx\}}\Bigg[|\Delta|^2 \\ &\quad + \left\{-\gamma^{\alpha}\left(i\partial_{\alpha} \pm \frac{1}{2}\tilde{e}\tilde{A}_{\alpha} + \bar{\mu}\,\delta_{\alpha 0}\right) - m\right\} \\ &\quad \times\left\{\gamma^{\alpha}\left(i\partial_{\alpha} \pm \frac{1}{2}\tilde{e}\tilde{A}_{\alpha} - \bar{\mu}\,\delta_{\alpha 0}\right) - m\right\}\Bigg],\end{aligned} \tag{3.7}$$

where we have skipped the superscript "ext" on the exter-

nal rotated gauge field $\tilde{A}_\mu$. Here, $\breve{\mu} \equiv \mu - 2\mu_8$, $\bar{\mu} \equiv \mu + \mu_8$, and $m \equiv m_0 + \sigma$. The determinants in (3.7) are now to be calculated in the momentum space. To do this, a generalization of the method described in [20] for arbitrary charges is necessary. This method is originally developed by Ritus in [35] in order to determine the Green's function of charged fermions in the presence of background magnetic field. It is then extended to charged vector fields in [36]. Recently, it is used in [37] to determine the electric-current susceptibility of quark matter in the presence of external constant magnetic field. As it is described in [37], in the Landau gauge for the external rotated gauge field, a projection operator P_n can be defined

$$\begin{aligned} P_n &\equiv \frac{1}{2}[f_{n_+}(x) + f_{n_-}(x)] + \frac{i}{2}[f_{n_+}(x) - f_{n_-}(x)]\gamma^1\gamma^2, \quad \text{for } qB > 0, \\ P_n &\equiv \frac{1}{2}[f_{n_+}(x) + f_{n_-}(x)] - \frac{i}{2}[f_{n_+}(x) - f_{n_-}(x)]\gamma^1\gamma^2, \quad \text{for } qB < 0, \end{aligned} \tag{3.8}$$

that includes the basis functions $f_{n_\pm}(x)$ defined by

$$\begin{aligned} f_{n_+}(x) &= \phi_n\Big(x - \frac{p_y}{qB}\Big), \qquad n = 0, 1, 2, \cdots, \\ f_{n_-}(x) &= \phi_{n-1}\Big(x - \frac{p_y}{qB}\Big), \qquad n = 1, 2, 3 \cdots. \end{aligned} \tag{3.9}$$

Here, $\phi_n(x)$ are the standard Landau quantized wave functions [37]

$$\phi_n(x) = \sqrt{\frac{1}{2^n n!}}\Big(\frac{|qB|}{\pi}\Big)^{1/4} \exp\Big(-\frac{1}{2}|qB|x^2\Big) H_n(\sqrt{|qB|}x), \tag{3.10}$$

with $H_n(x)$ the Hermite polynomial of degree n. Using the projectors P_n from (3.8), it is easy to show that

$$\begin{aligned} &\gamma_\mu(i\partial^\mu + qA^\mu)P_n e^{-i(p_0t - p_yy - p_zz)} \\ &= P_n(p_0\gamma^0 - \mathrm{sgn}(qB)\sqrt{2|qB|n}\gamma^2 - p_z\gamma^3)e^{-i(p_0t - p_yy - p_zz)}. \end{aligned} \tag{3.11}$$

The r.h.s. of (3.11) is a free Dirac operator with a modified momentum

$$\bar{p}^{\,\mu} = (p_0, 0, \mathrm{sgn}(qB)\sqrt{2|qB|n}, p_3). \tag{3.12}$$

This shows also that the solution of the Dirac equation in the presence of a constant magnetic field can be given by a combination of the projection operators P_n and the ordinary free Dirac spinors $u(p, s)$ and $v(p, s)$ [37].

To compute the determinants in (3.7) in the momentum space, we will use, for the charges $\tilde{q} \neq 0$, an appropriate momentum basis, similar to (3.12), and for $\tilde{q} = 0$, the ordinary four-momentum p^μ. In other words, we have

$$\begin{aligned} \bar{p}^{\,\mu}_{\tilde{q}\neq 0} &= \Big(p_0, 0, \frac{\tilde{q}}{|\tilde{q}|}\sqrt{2|\tilde{q}\,\tilde{e}\,B|n}, p_3\Big), \quad \text{for } \tilde{q} = 1, \pm\frac{1}{2}, \\ \bar{p}^{\,\mu}_{\tilde{q}=0} &= (p_0, p_1, p_2, p_3), \quad \text{for } \tilde{q} = 0, \end{aligned} \tag{3.13}$$

where $\frac{\tilde{q}}{|\tilde{q}|}$ replaces $\mathrm{sgn}(\tilde{q}B)$ in (3.12). This leads to the well-known quasiparticle dispersion relations in the presence of a constant magnetic field aligned in the third direction [23],

$$\begin{aligned} E_{\tilde{q}} &= \sqrt{2|\tilde{q}\,\tilde{e}\,B|n + p_3^2 + m^2} \quad \text{for } \tilde{q} = 1, \pm\frac{1}{2}, \\ E_0 &= \sqrt{p_1^2 + p_2^2 + p_3^2 + m^2} \quad \text{for } \tilde{q} = 0. \end{aligned} \tag{3.14}$$

Using the momenta (3.13) and transforming (3.4) and (3.5) into the Fourier space, the one-loop effective action reads

$$\tilde{\Gamma}^{(1)}_{\mathrm{eff}}(\bar{p}) = \sum_{\kappa\in\{r,g,b\}} \tilde{\Gamma}^{(1)/\kappa}_{\mathrm{eff}}(\bar{p}), \tag{3.15}$$

with

$$\begin{aligned} \tilde{\Gamma}^{(1)/b}_{\mathrm{eff}}(\bar{p}) &= -i\sum_{\tilde{q}\in\{0,1\}} \mathrm{lndet}_x[\{(E_{\tilde{q}} + \breve{\mu})^2 - p_0^2\}\{(E_{\tilde{q}} - \breve{\mu})^2 - p_0^2\}], \\ \sum_{\kappa\in\{r,g\}} \tilde{\Gamma}^{(1)/\kappa}_{\mathrm{eff}}(\bar{p}) &= -2i\sum_{\tilde{q}\in\{+1/2,-1/2\}} \mathrm{lndet}_x[(E^{(+)2}_{\tilde{q}} - p_0^2)(E^{(-)2}_{\tilde{q}} - p_0^2)]. \end{aligned} \tag{3.16}$$

Here, $E_{\tilde{q}}$ for $\tilde{q} \in \{0, 1, \pm\frac{1}{2}\}$ are defined in (3.14), and $E^{(\pm)}_{\tilde{q}} \equiv \sqrt{(E_{\tilde{q}} \pm \bar{\mu})^2 + |\Delta|^2}$, for $\tilde{q} \in \{+\frac{1}{2}, -\frac{1}{2}\}$. The factor 2 in the last equation of (3.16) reflects the degeneracy in the quark charges for $u_{r/g}$ as well as $d_{r/g}$ (see Table I). Note that a trace over Landau levels, n, is implemented in the expression on the r.h.s. of (3.16). This is because $E_{\tilde{q}\neq 0}$ from (3.14) depends explicitly on n. This trace will be performed in the next step, where the one-loop effective action will be explicitly determined in the momentum space. Performing the remaining determinant in the coordinate space leads, for a constant background magnetic field, to a space-time volume $\mathcal{V}$. At this stage, we will introduce the effective thermodynamic (mean field) potential Ω_{eff}, that is defined

by the effective action through the relation $\Gamma_{\rm eff} = -\mathcal{V}\Omega_{\rm eff}$. To determine the one-loop contribution to the one-loop effective potential at zero temperature $\Omega^{(1)}_{\rm eff}$, it is convenient to determine it first at finite temperature, and then taking the limit $T \to 0$, consider only the zero temperature effects [23]. For quarks with $\tilde{q} = 0$, one replaces p_0 by $p_0 = i\omega_\ell$,[10] where ω_ℓ are the Matsubara frequency defined by $\omega_\ell \equiv (2\ell + 1)\pi T$, and the p_0 integration by an infinite sum over the Matsubara frequencies. For an arbitrary function $f(p_0, \bar{\mathbf{p}}_{\tilde{q}})$, we get therefore

$$\int \frac{d^4p}{(2\pi)^4} f(p_0, \bar{\mathbf{p}}_{\tilde{q}=0}) = \frac{1}{\beta} \sum_{\ell=-\infty}^{+\infty} \int \frac{d^3p}{(2\pi)^3} f(i\omega_\ell, \mathbf{p}), \tag{3.17}$$

where $\beta \equiv T^{-1}$ is the inverse of the temperature T. For the quarks with $\tilde{q} \neq 0$, apart from a summation over the Matsubara frequencies ℓ, a summation over the Landau levels n is also to be considered [see (3.13)]. We get therefore [33]

$$\int \frac{d^4p}{(2\pi)^4} f(p_0, \bar{\mathbf{p}}_{\tilde{q}\neq 0}) = \frac{|\tilde{q}\,\tilde{e}\,B|}{\beta} \sum_{\ell=-\infty}^{+\infty} \sum_{n=0}^{+\infty} \alpha_n \int_{-\infty}^{+\infty} \frac{dp_3}{8\pi^2} \times f(i\omega_\ell, n, p_3), \tag{3.18}$$

where $\alpha_n = 2 - \delta_{n0}$ reflects the fact that Landau levels with $n > 0$ are doubly degenerate [20,23]. Following the above recipe, the one-loop contribution to the thermodynamic potential is given by

$$\Omega^{(1)}_{\rm eff} = \sum_{\tilde{q}\in\{0,1,\pm 1/2\}} \Omega^{\tilde{q}}_{\rm eff}, \tag{3.19}$$

where for $\tilde{q} = 0$, we have

$$\begin{aligned}
\Omega^{\tilde{q}=0}_{\rm eff} &= i\mathcal{V}^{-1} \ln\det[\beta^4\{(E_0 + \breve{\mu})^2 + \omega_\ell^2\}\{(E_0 - \breve{\mu})^2 + \omega_\ell^2\}] \\
&= -\frac{1}{\beta} \sum_{\ell=-\infty}^{+\infty} \int \frac{d^3p}{(2\pi)^3} \ln[\beta^4\{(E_0 + \breve{\mu})^2 + \omega_\ell^2\}\{(E_0 - \breve{\mu})^2 + \omega_\ell^2\}] \\
&= -\frac{2}{\beta} \int \frac{d^3p}{(2\pi)^3} \{\beta E_0 + \ln(1 + e^{-\beta(E_0+\breve{\mu})}) + \ln(1 + e^{-\beta(E_0-\breve{\mu})})\},
\end{aligned} \tag{3.20}$$

and for $\tilde{q} = 1$, we have

$$\begin{aligned}
\Omega^{\tilde{q}=1}_{\rm eff} &= i\mathcal{V}^{-1} \ln\det[\beta^4\{(E_{+1} + \breve{\mu})^2 + \omega_\ell^2\}\{(E_{+1} - \breve{\mu})^2 + \omega_\ell^2\}] \\
&= -\frac{\tilde{e}B}{\beta} \sum_{\ell=-\infty}^{+\infty} \sum_{n=0}^{+\infty} \alpha_n \int_{-\infty}^{+\infty} \frac{dp_3}{8\pi^2} \ln[\beta^4\{(E_{+1} + \breve{\mu})^2 + \omega_\ell^2\}\{(E_{+1} - \breve{\mu})^2 + \omega_\ell^2\}] \\
&= -\frac{2\tilde{e}B}{\beta} \sum_{n=0}^{+\infty} \alpha_n \int_{-\infty}^{+\infty} \frac{dp_3}{8\pi^2} \{\beta E_{+1} + \ln(1 + e^{-\beta(E_{+1}+\breve{\mu})}) + \ln(1 + e^{-\beta(E_{+1}-\breve{\mu})})\}.
\end{aligned} \tag{3.21}$$

Note that E_{+1} depends explicitly on n that labels the Landau levels. Finally, for $\tilde{q} = \pm\frac{1}{2}$, we arrive at

$$\begin{aligned}
\sum_{\tilde{q}\in\{+1/2,-1/2\}} \Omega^{\tilde{q}}_{\rm eff} &= 4i\mathcal{V}^{-1} \ln\det[\beta^4\{{E^+_{+1/2}}^2 + \omega_\ell^2\}\{{E^-_{+1/2}}^2 + \omega_\ell^2\}] \\
&= -\frac{4\tilde{e}B}{\beta} \sum_{\ell=-\infty}^{+\infty} \sum_{n=0}^{+\infty} \alpha_n \int_{-\infty}^{+\infty} \frac{dp_3}{16\pi^2} \ln[\beta^4\{{E^+_{+1/2}}^2 + \omega_\ell^2\}\{{E^-_{+1/2}}^2 + \omega_\ell^2\}] \\
&= -\frac{4\tilde{e}B}{\beta} \sum_{n=0}^{+\infty} \alpha_n \int_{-\infty}^{+\infty} \frac{dp_3}{16\pi^2} \{\beta(|E^+_{+1/2}| + |E^-_{+1/2}|) + 2\ln(1 + e^{-\beta E^+_{+1/2}}) + 2\ln(1 + e^{-\beta E^-_{+1/2}})\}.
\end{aligned} \tag{3.22}$$

where $E^+_{+1/2} = E^+_{-1/2}$ and $E^-_{+1/2} = E^-_{-1/2}$ are used. Plugging (3.20)–(3.22) in (3.19) and taking the limit $T \to 0$ by making use of the relation [38]

$$\lim_{T\to 0} T \ln[1 + e^{-x/T}] = -x\theta(-x), \tag{3.23}$$

with $\theta(x)$ is the Heaviside θ-function, the temperature independent part of the effective potential, including the tree level and the one-loop corrections reads

[10]The effect of the chemical potential is already considered in $\Gamma^{(1)}_{\rm eff}$ as well as $\Omega^{(1)}_{\rm eff}$.

$$\begin{aligned}\Omega_{\text{eff}} &= \Omega^{(0)} + \Omega^{(1)}_{\text{eff}} \\ &= \frac{\sigma^2}{4G_S} + \frac{|\Delta|^2}{4G_D} + \frac{B^2}{2} - 2\int_{-\infty}^{+\infty}\frac{d^3p}{(2\pi)^3}[E_0 - (E_0 - \breve{\mu})\theta(\breve{\mu} - E_0) - (\breve{\mu} + E_0)\theta(-\breve{\mu} - E_0)] \\ &\quad - \tilde{e}B\sum_{n=0}^{+\infty}\alpha_n\int_{-\infty}^{+\infty}\frac{dp_3}{4\pi^2}[E_{+1} + E^+_{+1/2} + E^-_{+1/2} + (\breve{\mu} - E_{+1})\theta(\breve{\mu} - E_{+1}) - 2E^+_{+1/2}\theta(-E^+_{+1/2}) \\ &\quad - 2E^-_{+1/2}\theta(-E^-_{+1/2}) - (\breve{\mu} + E_{+1})\theta(-\breve{\mu} - E_{+1})].\end{aligned} \tag{3.24}$$

The above result (3.24) is comparable with the result in [6], which is derived for a similar 2SC model in the absence of the magnetic field $\tilde{\mathbf{B}}$. In this case the thermodynamic potential up to one-loop order at finite T is given by

$$\hat{\Omega}_{\text{eff}} = \frac{\sigma^2}{4G_S} + \frac{|\Delta|^2}{4G_D} + \sum_{\kappa\in\{r,g,b\}}\hat{\Omega}^{(1)/\kappa}_{\text{eff}}, \tag{3.25}$$

where for different colors, we have

$$\begin{aligned}\hat{\Omega}^{(1)/b}_{\text{eff}} &= -2i\mathcal{V}^{-1}\,\text{lndet}[(\breve{E}^2_+ + \omega^2_\ell)(\breve{E}^2_- + \omega^2_\ell)] = -\frac{2}{\beta}\sum_{\ell=-\infty}^{+\infty}\int\frac{d^3p}{(2\pi)^3}\ln[\beta^4(\breve{E}^2_+ + \omega_\ell{}^2)(\breve{E}^2_- + \omega_\ell{}^2)] \\ &= -\frac{4}{\beta}\int\frac{d^3p}{(2\pi)^3}\{\beta E + \ln(1 + e^{-\beta(E+\breve{\mu})}) + \ln(1 + e^{-\beta(E-\breve{\mu})})\},\end{aligned} \tag{3.26}$$

and

$$\begin{aligned}\sum_{\kappa\in\{r,g\}}\hat{\Omega}^{(1)/\kappa}_{\text{eff}} &= -4i\mathcal{V}^{-1}\,\text{lndet}[(E^{\Delta\,2}_+ + \omega_\ell{}^2)(E^{\Delta\,2}_- + \omega_\ell{}^2)] = -\frac{4}{\beta}\sum_{\ell=-\infty}^{+\infty}\int\frac{d^3p}{(2\pi)^3}\ln[\beta^4(E^{\Delta\,2}_+ + \omega_\ell{}^2)(E^{\Delta\,2}_- + \omega_\ell{}^2)] \\ &= -\frac{4}{\beta}\int\frac{d^3p}{(2\pi)^3}\{\beta E^\Delta_- + \beta E^\Delta_+ + 2\ln(1 + e^{-\beta E^\Delta_-}) + 2\ln(1 + e^{-\beta E^\Delta_+})\},\end{aligned} \tag{3.27}$$

with $E \equiv \sqrt{\mathbf{p}^2 + m^2}$, $\breve{E}_\pm \equiv E \pm \breve{\mu}$, and $E^\Delta_\pm \equiv \sqrt{(E \pm \bar{\mu})^2 + |\Delta|^2}$. Using (3.23), the temperature independent part of (3.25) reads

$$\begin{aligned}\hat{\Omega}_{\text{eff}} &= \frac{\sigma^2}{4G_S} + \frac{|\Delta|^2}{4G_D} - 4\int\frac{d^3p}{(2\pi)^3}[E^\Delta_+ + E^\Delta_- + E + (\breve{\mu} - E)\theta(\breve{\mu} - E) - 2E^\Delta_-\theta(-E^\Delta_-) - 2E^\Delta_+\theta(-E^\Delta_+) \\ &\quad - (\breve{\mu} + E)\theta(-\breve{\mu} - E)].\end{aligned} \tag{3.28}$$

IV. ANALYTICAL SOLUTIONS OF THE χSB AND CSC GAP EQUATIONS IN THE LLL APPROXIMATION: A COMPARISON OF $B = 0$ AND $B \neq 0$ CASES

In the previous section, the one-loop effective action of the NJL model including meson (σ) and diquark (Δ) condensates in the 2SC phase at finite $\tilde{e}B$, μ and μ_8 is computed in the mean field approximation. This is the purpose of this paper to have a complete understanding on the effect of external magnetic field on the formation of these condensates. To this purpose one has to solve the following gap equations and color neutrality conditions

$$\begin{aligned}&\frac{\partial\Omega_{\text{eff}}(\sigma,\Delta,\mu_8;\mu,\tilde{e}B)}{\partial\sigma}\bigg|_{\sigma_B,\Delta_B,\mu_8} = 0, \\ &\frac{\partial\Omega_{\text{eff}}(\sigma,\Delta,\mu_8;\mu,\tilde{e}B)}{\partial\Delta}\bigg|_{\sigma_B,\Delta_B,\mu_8} = 0, \\ &\frac{\partial\Omega_{\text{eff}}(\sigma,\Delta,\mu_8;\mu,\tilde{e}B)}{\partial\mu_8}\bigg|_{\sigma_B,\Delta_B,\mu_8} = 0.\end{aligned} \tag{4.1}$$

The solutions of the first two equations build the ''local'' minima of the theory. In Sec. IV, we will solve the above equations numerically for any value of the rotated magnetic field $\tilde{e}B$. Keeping $(\sigma,\Delta) \neq (0,0)$ and looking for global minima for the system described by complete

$\Omega_{\rm eff}(\sigma, \Delta, \mu_8; \mu, \tilde{e}B)$ from (3.24) in the presence of the rotated field, it turns out that in the regime $300 \lesssim \mu \lesssim 500$ MeV, the system exhibits two "global" minima. They are given by $(\sigma_B \neq 0, \Delta_B = 0, \mu_8 = 0)$ in the regime $\mu < \mu_c$, and $(\sigma_B = 0, \Delta_B \neq 0, \mu_8 \neq 0)$ in the regime $\mu > \mu_c$. Here, μ_c is a certain critical chemical potential, and, shall be determined numerically in Sec. IV for a wide range of $\tilde{e}B$ [see Fig. 9]. We will denote the regime characterized by $(\sigma_B \neq 0, \Delta_B = 0, \mu_8 = 0)$ and $(\sigma_B = 0, \Delta_B \neq 0, \mu_8 \neq 0)$, by the χSB and the CSC phases, respectively. In this section, we will analytically determine the solutions of the above gap equations in the limit of strong magnetic fields $|\tilde{q}\,\tilde{e}\,B| \gg \mu^2$, and in the χSB and the CSC phases separately. We will then compare these solutions with the corresponding solutions of the gap equations in $B = 0$ case. In the above limit, the dynamics of the system is dominated by LLL. The goal is to determine analytically the mass gaps of the χSB and CSC phases separately. This will be done in Secs. IV A and IV B, respectively. In IV A 1 as well as IV B 1, we consider the case of strong magnetic field, whereas IV A 2 as well as IV B 2 are devoted to $B = 0$ case.

A. The chiral symmetry breaking phase

1. Strong magnetic field

According to the descriptions from the previous paragraph, the χSB phase is characterized by $\sigma_B \neq 0$ and $\Delta_B = \mu_8 = 0$. To study this phase in the LLL approximation, we will, in particular, focus on the first gap equation from (4.1)

$$\frac{\partial \Omega^{\rm LLL}_{\rm eff}(\sigma, \Delta, \mu_8; \mu, \tilde{e}B)}{\partial \sigma}\bigg|_{\sigma_B, \Delta_B = \mu_8 = 0} = 0, \tag{4.2}$$

or equivalently on[11]

$$\frac{\partial \Omega^{\rm LLL}_{\chi\rm SB}(\sigma, \Delta_B = \mu_8 = 0; \mu, \tilde{e}B)}{\partial \sigma}\bigg|_{\sigma_B} = 0, \tag{4.3}$$

where $\Omega^{\rm LLL}_{\chi\rm SB}$ arises from (3.24) with $n = 0$ and $(\sigma_B \neq 0, \Delta_B = \mu_8 = 0)$. To solve (4.3) analytically, let us consider $\Omega^{\rm LLL}_{\chi\rm SB}$ first in the momentum space

$$\begin{aligned}\Omega^{\rm LLL}_{\chi\rm SB}(\sigma, \Delta_B = \mu_8 = 0) &= \frac{\sigma^2}{4G_S} + \frac{B^2}{2} - 2\int \frac{d^3p}{(2\pi)^3}[\sqrt{p^2+\sigma^2} + (\mu - \sqrt{p^2+\sigma^2})\theta(\mu - \sqrt{p^2+\sigma^2})] \\ &\quad - 3\tilde{e}B\int_{-\infty}^{+\infty}\frac{dp_3}{4\pi^2}[\sqrt{p_3^2+\sigma^2} + (\mu - \sqrt{p_3^2+\sigma^2})\theta(\mu - \sqrt{p_3^2+\sigma^2})] \\ &= \frac{\sigma^2}{4G_S} + \frac{B^2}{2} - \left[\int_0^{\Lambda}\frac{p^2dp}{\pi^2}\sqrt{p^2+\sigma^2} + \theta(\mu-\sigma)\int_0^{\sqrt{\mu^2-\sigma^2}}\frac{p^2dp}{\pi^2}(\mu - \sqrt{p^2+\sigma^2})\right] \\ &\quad - 3\tilde{e}B\left[\int_0^{\Lambda_B}\frac{dp_3}{2\pi^2}\sqrt{{p_3}^2+\sigma^2} + \theta(\mu-\sigma)\int_0^{\sqrt{\mu^2-\sigma^2}}\frac{dp_3}{2\pi^2}(\mu - \sqrt{{p_3}^2+\sigma^2})\right].\end{aligned} \tag{4.4}$$

Here, we have introduced the momentum cutoff Λ for the first integral arising from the contribution of zero charged particle. In contrast, the momentum cutoff $\Lambda_B \equiv \sqrt{\tilde{e}B}$ is chosen for the first integral proportional to $\tilde{e}B$, that arises from the contribution of the remaining three charged particles.[12] Considering furthermore the effect of the Heaviside θ-functions in the integrations limits, the corresponding momentum cutoff to the remaining two integrals is given by $\sqrt{\mu^2-\sigma^2}$ with the assumption that $\sigma < \mu$ (see the $\theta(\mu-\sigma)$ before these two integrals). Performing the integrations over $p \equiv |\mathbf{p}|$ and p_3 in (4.4), we arrive at

$$\begin{aligned}\Omega^{\rm LLL}_{\chi\rm SB}(\sigma, \Delta_B = \mu_8 = 0) &= \frac{\sigma^2}{4G_S} + \frac{B^2}{2} + \frac{\sigma^4}{8\pi^2}\left[\ln\left(\frac{\Lambda + \sqrt{\Lambda^2+\sigma^2}}{\sigma}\right) - \theta(\mu-\sigma)\ln\left(\frac{\mu + \sqrt{\mu^2-\sigma^2}}{\sigma}\right)\right] \\ &\quad - \frac{\Lambda}{8\pi^2}\sqrt{\Lambda^2+\sigma^2}(2\Lambda^2+\sigma^2) - \frac{\mu}{24\pi^2}\theta(\mu-\sigma)\sqrt{\mu^2-\sigma^2}(2\mu^2-5\sigma^2) \\ &\quad - \frac{3\tilde{e}B\sigma^2}{4\pi^2}\left[\ln\left(\frac{\Lambda_B + \sqrt{\Lambda_B^2+\sigma^2}}{\sigma}\right) - \theta(\mu-\sigma)\ln\left(\frac{\mu + \sqrt{\mu^2-\sigma^2}}{\sigma}\right)\right] \\ &\quad - \frac{3\tilde{e}B}{4\pi^2}[\Lambda_B\sqrt{\Lambda_B^2+\sigma^2} + \theta(\mu-\sigma)\mu\sqrt{\mu^2-\sigma^2}].\end{aligned} \tag{4.5}$$

Minimizing the above potential according to (4.3), the gap equation reads

[11] In [8], the same procedure is performed to study the χSB and the CSC phases separately.

[12] The charges of the particles is defined with respect of the rotated magnetic field. They are presented in Table I, in units of $\tilde{e}$.

$$0 = \frac{\partial \Omega^{\mathrm{LLL}}_{\chi\mathrm{SB}}}{\partial \sigma}\bigg|_{\sigma=\sigma_B}$$
$$= \sigma_B\Big\{\frac{\pi^2}{G_S} - \Lambda\sigma_B\sqrt{\Lambda^2+\sigma_B^2} - 3\tilde{e}B\ln\Big(\frac{\Lambda_B+\sqrt{\Lambda_B^2+\sigma_B^2}}{\sigma_B}\Big) + \sigma_B^2\ln\Big(\frac{\Lambda+\sqrt{\Lambda^2+\sigma_B^2}}{\sigma_B}\Big)$$
$$+ \theta(\mu-\sigma_B)\Big[\mu\sqrt{\mu^2-\sigma_B^2} + (3\tilde{e}B-\sigma_B^2)\ln\Big(\frac{\mu+\sqrt{\mu^2-\sigma_B^2}}{\sigma_B}\Big)\Big]\Big\}. \tag{4.6}$$

To find a nontrivial solution $\sigma_B \neq 0$ to this equation, we expand it in the orders of the dimensionless and small parameter $x \equiv \frac{\sigma_B}{\Lambda} \ll 1$ up to order $\mathcal{O}(x^3)$, and get

$$2\Lambda^2\Big(\frac{1}{g_s}-1\Big) = \sigma_B^2\Big(\frac{5}{2}-\ln\Big(\frac{4\Lambda^2}{\sigma_B^2}\Big)\Big) + 3\tilde{e}B\ln\Big(\frac{4\Lambda_B^2}{\sigma_B^2}\Big) + \theta(\mu-\sigma_B)\Big\{\sigma_B^2 - 2\mu^2 + (\sigma_B^2-3\tilde{e}B)\ln\Big(\frac{4\mu^2}{\sigma_B^2}\Big)\Big\}, \tag{4.7}$$

where the dimensionless coupling $g_s \equiv \frac{G_S\Lambda^2}{\pi^2}$ is introduced. In what follows, we consider two different regimes of $\mu \leq \sigma_B$ and $\mu > \sigma_B$ separately. To find real solution for the simplified gap equation (4.7), we will then distinguish various regions for the dimensionless coupling g_s.

(i) In the first regime characterized by $\mu \leq \sigma_B$, the gap equation (4.7) reads

$$2\Lambda^2\Big(\frac{1}{g_s}-1\Big) = \frac{5\sigma_B^2}{2} - \sigma_B^2\ln\Big(\frac{4\Lambda^2}{\sigma_B^2}\Big) + 3\tilde{e}B\ln\Big(\frac{4\Lambda_B^2}{\sigma_B^2}\Big). \tag{4.8}$$

Since for $0 < g_s < 1$, the l.h.s. of (4.8) is positive, a nontrivial real solution arises only by the assumption $\sigma_B^2\ln(\frac{4\Lambda^2}{\sigma_B^2}) \ll 3\tilde{e}B\ln(\frac{4\Lambda_B^2}{\sigma_B^2})$, which is indeed justified in the LLL approximation. Neglecting, therefore, the first two terms on the r.h.s. of (4.8), we arrive at

$$\sigma_B^2 = 4\tilde{e}Be^{-(2\Lambda^2/3\tilde{e}B)[(1/g_s)-1]}. \tag{4.9}$$

Note that the assumption $\sigma_B^2\ln(\frac{4\Lambda^2}{\sigma_B^2}) \ll 3\tilde{e}B\ln(\frac{4\Lambda_B^2}{\sigma_B^2})$ does not set any limitation on the relation between two momentum cutoffs Λ and Λ_B. Depending on whether Λ is larger or smaller than Λ_B, different regimes are to be distinguished for the coupling g_s:

$$\text{For } \Lambda \leq \Lambda_B, \quad \text{we get} \quad 0 < g_s < \frac{\Lambda^2}{\Lambda^2 - 3\tilde{e}B\ln(\frac{\Lambda}{2\Lambda_B})} < 1,$$
$$\text{For } \Lambda > \Lambda_B, \quad \text{we get} \quad 0 < g_s < \frac{\Lambda^2}{\Lambda^2 + 3\tilde{e}B\ln 2} < 1. \tag{4.10}$$

The dynamical mass σ_B from (4.9) is, apart from numerical factors, the same as the dynamical mass of the NJL model in the presence of constant magnetic field from [28]. The additional factor $1/3$, that arises in the exponent of (4.9) corresponds to three different quark charges $\tilde{q} = 1, \pm\frac{1}{2}$ that have, in the regime of LLL dominance ($n = 0$) equal contributions to the effective potential in the χSB phase.

Let us consider again the gap equation (4.8) for the case $g_s > 1$. In this case a nontrivial solution may exist only for Λ in the same order of magnitude as Λ_B. To find the solution, we rewrite first the gap equation (4.8) as

$$2\Lambda^2\Big(\frac{1}{g_s}-1\Big) = -\sigma_B^2\ln\Big(\frac{4\Lambda^2}{e^{5/2}\sigma_B^2}\Big) + 3\tilde{e}B\Big(\ln\Big(\frac{3\Lambda_B^2}{2\Lambda^2}\Big) + \ln\Big(\frac{8\Lambda^2}{3\sigma_B^2}\Big)\Big). \tag{4.11}$$

Expanding now the second term on the r.h.s. in the orders of $y \equiv \frac{2\Lambda^2}{3\Lambda_B^2} - 1 \simeq 0$ up to $\mathcal{O}(y^2)$, we arrive at

$$2\Lambda^2\Big(\frac{1}{g_s}-1\Big) \approx -\sigma_B^2\ln\Big(\frac{4\Lambda^2}{e^{5/2}\sigma_B^2}\Big) - 3\tilde{e}B\Big(\frac{2\Lambda^2}{3\Lambda_B^2}-1\Big) + 3\tilde{e}B\ln\Big(\frac{8\Lambda^2}{3\sigma_B^2}\Big). \tag{4.12}$$

Using the same approximation $\sigma_B^2\ln(\frac{4\Lambda^2}{\sigma_B^2}) \ll 3\tilde{e}B\ln(\frac{4\Lambda_B^2}{\sigma_B^2})$, we can neglect the first term on the r.h.s. of (4.12), and arrive at

$$\frac{2\Lambda^2}{g_s} \approx 3\tilde{e}B\ln\Big(\frac{8\Lambda^2}{3\sigma_B^2}\Big) + 3\tilde{e}B, \tag{4.13}$$

whose solution reads

$$\sigma_B^2 = \mathcal{C}\Lambda^2 e^{-(2\Lambda^2/3\tilde{e}Bg_s)}, \quad \text{with} \quad \mathcal{C} = \tfrac{8}{3}e \approx 7.25. \tag{4.14}$$

(ii) In the regime characterized by $\sigma_B < \mu$, the gap equation is given by

$$\Lambda^2\Big(\frac{1}{g_s}-1\Big) = \frac{7\sigma_B^2}{4} - \mu^2 - \frac{3\tilde{e}B}{2}\ln\frac{\mu^2}{\Lambda_B^2} + \frac{\sigma_B^2}{2}\ln\frac{\mu^2}{\Lambda^2}. \tag{4.15}$$

It arises by expanding (4.6) in the orders of $x = \frac{\sigma_B}{\Lambda}$ up to order $\mathcal{O}(x^3)$. As it turns out a real solution may be found by expanding (4.15) in the orders $w \equiv \frac{\mu^2}{\Lambda^2} - 1 \simeq 0$ and $z \equiv \frac{\mu^2}{\Lambda_B^2} - 1 \simeq 0$ up to $\mathcal{O}(w^2)$ as well as $\mathcal{O}(z^2)$. The mass gap can

be computed directly from the resulting equation and reads

$$\sigma_B^2 \simeq \Lambda^2\left(\frac{1}{g_s}-1\right)-\frac{3\tilde{e}B}{2}+\frac{5\mu^2}{2}. \tag{4.16}$$

Note that a real solution for σ_B in this regimes arises only when $\tilde{e}B$ and g_s satisfy the following conditions:

$$\begin{aligned}\text{For } 0<g_s<1:&\begin{cases}\mu^2<\Lambda_B\le\frac{5\mu^2}{3}, & \text{and}\quad \frac{2\Lambda^2}{3\tilde{e}B+2\Lambda^2-3\mu^2}<g_s<1,\\ \frac{5\mu^2}{3}<\Lambda_B, & \text{and}\quad \frac{2\Lambda^2}{3\tilde{e}B+2\Lambda^2-3\mu^2}<g_s<\frac{2\Lambda^2}{3\tilde{e}B+2\Lambda^2-5\mu^2},\end{cases}\\ \text{For } g_s>1:&\left\{\mu^2<\Lambda_B<\frac{5\mu^2}{3}, \quad \text{and}\quad 1<g_s<\frac{2\Lambda^2}{3\tilde{e}B+2\Lambda^2-5\mu^2}.\right.\end{aligned} \tag{4.17}$$

The above conditions arise without specifying any relation between Λ and Λ_B.

2. Zero magnetic field

To clarify the effect of strong magnetic fields on the mass gap, we will present in what follows the analytical results of the gap equation corresponding to the effective potential (3.28) at zero magnetic field.[13] Setting, as in the previous section, in the χSB phase, $\Delta_0=\mu_8=0$ in the corresponding effective potential (3.28), the resulting potential in the momentum space reads

$$\begin{aligned}&\hat{\Omega}_{\chi\mathrm{SB}}(\sigma,\Delta_0=\mu_8=0)\\ &=\frac{\sigma^2}{4G_S}-6\int_0^\Lambda\frac{p^2dp}{\pi^2}(\sqrt{p^2+\sigma^2}+(\mu-\sqrt{p^2+\sigma^2})\\ &\quad\times\theta(\mu-\sqrt{p^2+\sigma^2})).\end{aligned} \tag{4.18}$$

After performing the p integration, we arrive at

$$\begin{aligned}\hat{\Omega}_{\chi\mathrm{SB}}(\sigma,\Delta_0=\mu_8=0)=&\frac{\sigma^2}{4G_S}+\frac{3m^4}{4\pi^2}\left[\ln\left(\frac{\Lambda+\sqrt{\Lambda^2+\sigma^2}}{\sigma}\right)-\theta(\mu-\sigma)\ln\left(\frac{\mu+\sqrt{\mu^2-\sigma^2}}{\sigma}\right)\right]\\ &-\frac{3\Lambda}{4\pi^2}(2\Lambda^2+\sigma^2)\sqrt{\Lambda^2+\sigma^2}+\frac{\mu}{4\pi^2}(5\sigma^2-2\mu^2)\theta(\mu-\sigma)\sqrt{\mu^2-\sigma^2}.\end{aligned} \tag{4.19}$$

The corresponding gap equation reads then

$$\begin{aligned}0=&\frac{\partial\hat{\Omega}_{\chi\mathrm{SB}}}{\partial\sigma}\bigg|_{\sigma=\sigma_0}\\ =&\frac{\pi^2}{6G_S}-\Lambda\sqrt{\Lambda^2+\sigma_0^2}+\sigma_0^2\ln\left(\frac{\Lambda+\sqrt{\Lambda^2+\sigma_0^2}}{\sigma_0}\right)+\theta(\mu-\sigma_0)\left[\mu\sqrt{\mu^2-\sigma_0^2}-\sigma_0^2\ln\left(\frac{\mu+\sqrt{\mu^2-\sigma_0^2}}{\sigma_0}\right)\right].\end{aligned} \tag{4.20}$$

Defining, similar to what we did in the $B\neq 0$ case, a dimensionless parameter $\hat{x}\equiv\frac{\sigma_0}{\Lambda}\ll 1$, and expanding the gap equation (4.20) in the orders of $\hat{x}$ up to $\mathcal{O}(\hat{x}^3)$, we arrive at

$$0=\frac{\partial\hat{\Omega}_{\chi\mathrm{SB}}}{\partial\sigma}\bigg|_{\sigma=\sigma_0}=2\Lambda^2\left(\frac{1}{\hat{g}_s}-1\right)-\sigma_0^2\left(1-\ln\frac{4\Lambda^2}{\sigma_0^2}\right)+\theta(\mu-\sigma_0)\left(-\sigma_0^2+2\mu^2-\sigma_0^2\ln\frac{4\mu^2}{\sigma_0^2}\right), \tag{4.21}$$

where we have introduced the dimensionless coupling $\hat{g}_s\equiv\frac{6G_S\Lambda^2}{\pi^2}=6g_s$. To find a real solution for the mass gap σ_0, we have to distinguish two different regimes of the chemical potential μ. They are characterized by $\mu\le\sigma_0$ and $\sigma_0<\mu$.

(i) In the first regime characterized by $\mu\le\sigma_0$, a real solution $\sigma_0<\Lambda$ arises only for $1<\hat{g}_s<\hat{g}_1$ with $\hat{g}_1\equiv\frac{1}{1-\ln 2}\simeq 3.26$. It reads

$$\sigma_0^2=4\Lambda^2\exp\left(W_{-1}\left(\frac{1}{2\hat{g}_s}-\frac{1}{2}\right)\right). \tag{4.22}$$

It corresponds to one of the two real branches of the Lambert $W(x)$ function, $W_0(x)$ and $W_{-1}(x)$, which is

[13] In [6] the full gap equations of the 2SC model including the mesons is solved numerically for $B=0$. As it turns out the system exhibits, as in $B\neq 0$ case, a phase transition from the χSB to the CSC phase. Here, the χSB phase is characterized by $(\sigma_0\neq 0,\Delta_0=0)$ and the CSC by $(\sigma_0=0,\Delta_0\neq 0)$.

known to be the function satisfying (see [39] for more details on the Lambert W-function).[14]

$$W(x)e^{W(x)} = x. \tag{4.23}$$

(ii) In the second regime characterized by $\sigma_0 < \mu$, the gap equation is

$$\Lambda^2\left(\frac{1}{\hat{g}_s} - 1\right) = \sigma_0^2 - \mu^2 + \frac{\sigma_0^2}{2}\ln\left(\frac{\mu^2}{\Lambda^2}\right). \tag{4.24}$$

It arises from (4.20) by an expansion in the orders of $\hat{x} = \frac{\sigma_0}{\Lambda}$ up to $\mathcal{O}(\hat{x}^3)$. Introducing a small parameter $\hat{w} \equiv \frac{\mu^2}{\Lambda^2} - 1$ and expanding (4.24) in the orders of $\hat{w}$ up to $\mathcal{O}(\hat{w}^2)$, yields the mass gap

$$\sigma_0^2 = 2\Lambda^2\left(\frac{1}{\hat{g}_s} - 1\right) + 2\mu^2. \tag{4.25}$$

Note that a real solution for σ_0 arises only for $\hat{g}_s > 1$, satisfying

$$\frac{2\Lambda^2}{2\Lambda^2 - \mu^2} < \hat{g}_s < \frac{\Lambda^2}{\Lambda^2 - \mu^2}. \tag{4.26}$$

In Sec. V, we will perform a numerical analysis to study the χSB phase for any arbitrary magnetic field. We will show that, similar to the $B \neq 0$ case, the second regime characterized by $\sigma_0 < \mu$ belongs to the color symmetry breaking phase and is indeed irrelevant for the present χSB phase. Comparing therefore only the relevant part of the solutions, i.e. (4.9) for $B \neq 0$ with (4.22) for $B = 0$, we note that, in contrast to $B = 0$ case, in the presence of strong magnetic fields, the formation of chiral symmetry breaking bound state σ_B is possible even for small dimensionless χSB coupling $0 < g_s < 1$. This is in fact one of the consequences of the phenomenon of magnetic catalysis [28].

B. The color superconducting phase

1. Strong magnetic field

According to our explanation in the paragraph below (4.1), the CSC phase is characterized by ($\sigma_B = 0$, $\Delta \neq 0$, $\mu_8 \neq 0$). The corresponding effective potential arises from (3.24) by setting $n = 0$, and $\sigma_B = 0$. In the momentum space, it is given by

$$\begin{aligned}\Omega^{\mathrm{LLL}}_{\mathrm{CSC}}(\sigma_B = 0, \Delta, \mu_8) = {} & \frac{\Delta^2}{4G_D} + \frac{B^2}{2} - 2\int_0^\infty \frac{d^3p}{(2\pi)^3}[p + (\breve{\mu} - p)\theta(\breve{\mu} - p) - (\breve{\mu} + p)\theta(-\breve{\mu} - p)] \\ & - \tilde{e}B\int_0^\infty \frac{dp_3}{2\pi^2}[p_3 + (\breve{\mu} - p_3)\theta(\breve{\mu} - p_3) - (\breve{\mu} + p_3)\theta(-\breve{\mu} - p_3) + \sqrt{(p_3 + \bar{\mu})^2 + \Delta^2} \\ & + \sqrt{(p_3 - \bar{\mu})^2 + \Delta^2}].\end{aligned} \tag{4.27}$$

Performing the p_3 and p integrations by introducing the momentum cutoffs Λ and Λ_B for the $p = |\mathbf{p}|$ as well as p_3 integrations,[15] we arrive at

$$\begin{aligned}\Omega^{\mathrm{LLL}}_{\mathrm{CSC}}(\sigma_B = 0, \Delta, \mu_8) = {} & \frac{\Delta^2}{4G_D} + \frac{B^2}{2} - \frac{3\Lambda^4 + (3\tilde{e}B + \breve{\mu}^2)\breve{\mu}^2}{12\pi^2} - \frac{\tilde{e}B}{4\pi^2}\Big[\Lambda_B^2 + (\Lambda_B - \bar{\mu})\sqrt{\Delta^2 + (\Lambda_B - \bar{\mu})^2} \\ & + (\Lambda_B + \bar{\mu})\sqrt{\Delta^2 + (\Lambda_B + \bar{\mu})^2} + \Delta^2\ln\left(\frac{\sqrt{\Delta^2 + (\Lambda_B + \bar{\mu})^2} + (\Lambda_B + \bar{\mu})}{\sqrt{\Delta^2 + (\Lambda_B - \bar{\mu})^2} - (\Lambda_B - \bar{\mu})}\right)\Big].\end{aligned} \tag{4.28}$$

In the CSC phase, we have a set of two coupled equations: the color neutrality condition, $\frac{\partial\Omega^{\mathrm{LLL}}_{\mathrm{CSC}}}{\partial\mu_8} = 0$, and the gap equation $\frac{\partial\Omega^{\mathrm{LLL}}_{\mathrm{CSC}}}{\partial\Delta} = 0$. The goal is to solve these two equations to determine μ_8 and Δ as a function of the external magnetic field B and the chemical potential μ. Let us first consider the color neutrality condition

$$0 = \frac{\partial\Omega^{\mathrm{LLL}}_{\mathrm{CSC}}}{\partial\mu_8}\Big|_{\Delta_B} = 4\breve{\mu}^3 + 3\tilde{e}B(2\breve{\mu} + \sqrt{\Delta_B^2 + (\Lambda_B - \bar{\mu})^2} - \sqrt{\Delta_B^2 + (\Lambda_B + \bar{\mu})^2}), \tag{4.29}$$

where $\bar{\mu} = \mu + \mu_8$ and $\breve{\mu} = \mu - 2\mu_8$. Defining three dimensionless (small) parameters, $x \equiv \frac{\mu}{\Lambda}$, $y \equiv \frac{\Delta_B}{\Lambda}$, as well as $z \equiv \frac{\mu_8}{\Lambda}$, and expanding (4.29) in the orders of x, y and z up to $\mathcal{O}(x^4)$, $\mathcal{O}(y^3)$, and $\mathcal{O}(z^2)$, μ_8 can be determined from the resulting equation and is given by

$$\mu_8 = \frac{2\mu^3}{3(3\tilde{e}B + 4\mu^2)}. \tag{4.30}$$

As for the gap equation corresponding to Δ_B, we have

[14] According to the explanations in [39]: If x is real, then for $-1/e \leq x < 0$, there are two possible real values of $W(x)$. One denotes the branch satisfying $-1 \leq W(x)$ by $W_0(x)$, and the branch satisfying $W(x) \leq -1$ by $W_{-1}(x)$.

[15] See our description below (4.4) for the choice of the momentum cutoffs.

$$0 = \frac{\Omega_{\rm CSC}^{\rm LLL}}{\partial\Delta}\Big|_{\Delta_B} = \frac{\pi^2}{G_D} - \tilde{e}B\ln\Big(\frac{\sqrt{\Delta_B^2 + (\Lambda+\bar{\mu})^2} + (\Lambda_B + \bar{\mu})}{\sqrt{\Delta_B^2 + (\Lambda_B - \bar{\mu})^2} - (\Lambda_B - \bar{\mu})}\Big). \tag{4.31}$$

After expanding (4.31) in the orders of $y \equiv \frac{\Delta_B}{\Lambda}$ and $z \equiv \frac{\mu_8}{\Lambda}$ up to $\mathcal{O}(y^3)$ and $\mathcal{O}(z^2)$, and replacing μ_8 from (4.30) in the resulting equation, we arrive at

$$\frac{\Lambda^2}{g_d} + \frac{4\mu^4}{9\tilde{e}B} - \tilde{e}B\ln\Big(\frac{4(\tilde{e}B-\mu^2)}{\Delta_B^2}\Big) = 0, \tag{4.32}$$

where the dimensionless diquark coupling in the CSC phase $g_d \equiv \frac{G_D\Lambda^2}{\pi^2}$ is introduced. The diquark mass gap Δ_B can then be determined directly from (4.32) and reads

$$\Delta_B^2 = 4(\Lambda_B^2 - \mu^2)\exp\Big(-\frac{\Lambda^2}{\tilde{e}B}\frac{1}{g_d}\Big). \tag{4.33}$$

This result is comparable with the results by [20] for the three-flavor CFL model. In particular, in both models the exponents are proportional to $(\tilde{e}Bg_d)^{-1}$. The dependence of Δ_B on the magnetic field demonstrates the effect of magnetic catalysis [28], that states that even for small value of the dimensionless diquark coupling g_d, the presence of a strong magnetic field leads to color symmetry breaking and the formation of diquark mass Δ_B.

2. Zero magnetic field

We consider, as next, the effective potential of the 2SC model in the absence of magnetic field from (3.28) in the CSC phase by setting ($\sigma_0 = 0$, $\Delta_0 \neq 0$, $\mu_8 \neq 0$). In the momentum space, the resulting potential is then given by

$$\begin{aligned}\hat{\Omega}_{\rm CSC}(\sigma_0=0,\Delta,\mu_8) &= \frac{\Delta^2}{4G_D} - 2\int_0^\Lambda \frac{p^2dp}{\pi^2}[\sqrt{\Delta^2+(p+\bar{\mu})^2} + \sqrt{\Delta^2+(p-\bar{\mu})^2} + p + (\breve{\mu}-p)\theta(\breve{\mu}-p)\\ &\quad - (\breve{\mu}+p)\theta(-\breve{\mu}-p)] = \frac{\Delta^2}{4G_D} - \frac{\breve{\mu}^4}{6\pi^2} - \frac{\Lambda^4}{2\pi^2} - \frac{1}{12\pi^2}[3\Lambda(\Delta^2+2\Lambda^2) + \bar{\mu}(13\Delta^2-2\Lambda^2)\\ &\quad - 2\bar{\mu}^2(\Lambda+\bar{\mu})]\sqrt{\Delta^2+(\Lambda-\bar{\mu})^2} + [3\Lambda(\Delta^2+2\Lambda^2) - \bar{\mu}(13\Delta^2-2\Lambda^2) - 2\bar{\mu}^2(\Lambda-\bar{\mu})]\\ &\quad \times\sqrt{\Delta^2+(\Lambda+\bar{\mu})^2} - 3\Delta^2(\Delta^2-4\bar{\mu}^2)\\ &\quad \times\ln\Big(\frac{[\Lambda+\bar{\mu}+\sqrt{\Delta^2+(\Lambda+\bar{\mu})^2}][\Lambda-\bar{\mu}+\sqrt{\Delta^2+(\Lambda-\bar{\mu})^2}]}{\Delta^2}\Big).\end{aligned} \tag{4.34}$$

In this case, the color neutrality condition reads

$$\begin{aligned}0 &= \frac{\partial\hat{\Omega}_{\rm CSC}}{\partial\mu_8}\Big|_{\Delta_0,\hat{\mu}_8}\\ &= 2\breve{\mu}^3 - 3\Delta_0^2\bar{\mu}\ln\Big(\frac{[\Lambda+\bar{\mu}+\sqrt{\Delta_0^2+(\Lambda+\bar{\mu})^2}][\Lambda-\bar{\mu}+\sqrt{\Delta_0^2+(\Lambda-\bar{\mu})^2}]}{\Delta_0^2}\Big) - [2\Delta_0^2 - \Lambda^2 - \bar{\mu}(\Lambda+\bar{\mu})]\\ &\quad\times\sqrt{\Delta_0^2+(\Lambda-\bar{\mu})^2} + [2\Delta_0^2 - \Lambda^2 + \bar{\mu}(\Lambda-\bar{\mu})]\sqrt{\Delta_0^2+(\Lambda+\bar{\mu})^2}.\end{aligned} \tag{4.35}$$

After expanding (4.35) in the orders of $\hat{x} \equiv \frac{\mu}{\Lambda}$, $\hat{y} \equiv \frac{\Delta_0}{\Lambda}$, and $\hat{z} \equiv \frac{\hat{\mu}_8}{\Lambda}$ up to order $\mathcal{O}(\hat{x}^4)$, $\mathcal{O}(\hat{y}^3)$, as well as $\mathcal{O}(\hat{z}^2)$, we arrive at

$$\hat{\mu}_8 = \frac{\Delta_0^2}{3\mu} + \frac{\Delta_0^2}{6\mu}\ln\Big(\frac{\Delta_0^2}{4\Lambda^2}\Big), \tag{4.36}$$

where Δ_0 satisfies the gap equation

$$\begin{aligned}0 &= \frac{\hat{\Omega}_{\rm CSC}}{\partial\Delta}\Big|_{\Delta_0,\hat{\mu}_8}\\ &= -\frac{\pi^2}{2G_D} + (\Lambda+3\bar{\mu})\sqrt{\Delta_0^2+(\Lambda-\bar{\mu})^2} + (\Lambda-3\bar{\mu})\sqrt{\Delta_0^2+(\Lambda+\bar{\mu})^2} - (\Delta_0^2-2\bar{\mu}^2)\\ &\quad\times\ln\Big(\frac{[\Lambda+\bar{\mu}+\sqrt{\Delta_0^2+(\Lambda+\bar{\mu})^2}][\Lambda-\bar{\mu}+\sqrt{\Delta_0^2+(\Lambda-\bar{\mu})^2}]}{\Delta_0^2}\Big).\end{aligned} \tag{4.37}$$

Using the same method as above and expanding (4.37) in the orders of $\hat{y}$ and $\hat{z}$ up to order $\mathcal{O}(\hat{y}^3)$, as well as $\mathcal{O}(\hat{z}^2)$, we get

$$0 = \frac{\hat{\Omega}_{\mathrm{CSC}}}{\partial\Delta}\Big|_{\Delta_0,\hat{\mu}_8} = \Lambda^2\left(1-\frac{1}{\hat{g}_d}\right) - 3\mu^2 - \mu^2\ln\left(\frac{\Delta_0^2}{4(\Lambda^2-\mu^2)}\right), \quad (4.38)$$

where $\hat{g}_d \equiv \frac{4G_D\Lambda^2}{\pi^2} = 4g_d$. Solving (4.38), the diquark mass for vanishing magnetic fields is then given by

$$\Delta_0^2 = \mathcal{C}_2(\Lambda^2-\mu^2)\exp\left(-\frac{\Lambda^2}{\mu^2}\left(\frac{1}{\hat{g}_d}-1\right)\right), \quad \text{with}$$
$$\mathcal{C}_2 = 4e^{-3} \simeq 0.2. \quad (4.39)$$

The qualitative behavior of Δ_0 as a function of μ coincides with the results from [6,40]. The color chemical potential $\hat{\mu}_8$ arises by replacing (4.39) in (4.36). These results are to be compared with (4.33) [for the diquark mass gap Δ_B] as well as (4.30) [for the color chemical potential μ_8] in the presence of strong magnetic field.

V. NUMERICAL RESULTS FOR ARBITRARY MAGNETIC FIELD

In the previous section, we have presented analytical solutions for the order parameters σ and Δ corresponding to χSB and CSC phases, as well as for the color chemical potential μ_8 in the presence of strong magnetic fields in the LLL approximation. We have then compared our results with the mass gaps arising from the thermodynamic potential of the 2SC model in the absence of magnetic field in order to emphasize the effect of strong magnetic fields on the formation of bound states σ and Δ in the superconducting 2SC model. In this section, we will study numerically the effect of any arbitrary magnetic field on quark matter without restricting ourselves to LLL approximation. In particular, we are interested on the dependence of the mass gaps on the external magnetic field $\tilde{e}B$ and the chemical potential μ. To do this, we set, as in the previous section, $m_0 = 0$ and choose $G_D < G_S$. Comparing our numerical results with the analytical results from Sec. IV, we will determine numerically the range of the magnetic field strength for which the LLL approximation is reliable. At the end of this section, we will study the phase diagram of the model in a μ_c-$\tilde{e}B$ plane, and determine the type of various phase transitions between the χSB and the CSC phases for a wide range of $\tilde{e}B$.

Let us start with the one-loop effective potential (3.24) arising from a mean field approximation in the presence of an arbitrary magnetic field. To perform the momentum integrations numerically, we have to fix the free parameters of the model, the momentum cutoff Λ and the couplings G_S and G_D. Our specific choice of the parameters is [10]

$$\Lambda = 0.6533\ \mathrm{GeV}, \qquad G_S = 5.0163\ \mathrm{GeV}^{-2}, \quad \text{and} \quad G_D = \tfrac{3}{4}G_S. \quad (5.1)$$

For vanishing magnetic field $\tilde{e}B = 0$, they yield the χSB gap $\sigma_0 \simeq 323.8$ MeV at $\mu = 250$ MeV, and the 2SC gap of $\Delta_0 \simeq 126$ MeV at $\mu = 460$ MeV.[16] Smooth cutoff functions (form factor)

$$f_\Lambda = \frac{1}{1+\exp(\frac{|\mathbf{p}|-\Lambda}{A})}, \quad \text{and}$$
$$f^n_{\Lambda,B} = \frac{1}{1+\exp(\frac{\sqrt{p_3^2+2|\tilde{q}\,\tilde{e}\,B|n}-\Lambda}{A})}, \quad (5.2)$$

are then introduced to perform numerically the momentum p integrations corresponding to zero charged particles and charged particles, respectively.[17] In (5.3), A is a free parameter and is chosen to be $A = 0.05\Lambda$. Similar smooth cutoff function (form factor) is also used in [22]. Here, as in [22], the free parameter A determines the sharpness of the cutoff scheme. In what follows, we will first study the behavior of mass gaps as well as magnetizations in the χSB and CSC regimes as functions of $\tilde{e}B$ and for fixed chemical potentials.

In Fig. 1(a), the χSB mass gap σ is plotted as a function of $\tilde{e}B$ and for fixed chemical potential $\mu = 250$ MeV. Small oscillations for small value of $\tilde{e}B$ arise from the well-known van Alfven–de Haas (vAdH) effect [24]. They occur when the Landau levels pass the quark Fermi surface. They are also observed in [32] for the χSB mass gaps. Note that the oscillations are sharper, the smaller the value of the free parameter A in (5.3) is chosen [see also [41] for a discussion on the effect of free parameters in smooth cutoff functions (form factors)].[18] As for $\tilde{e}B \gtrsim 0.45\ \mathrm{GeV}^2$, where the dependence of σ_B on $\tilde{e}B$ is almost linear, we enter in the regime of LLL dominance. The qualitative behavior of σ_B as a function of $\tilde{e}B$ for strong magnetic fields can be checked by comparing our numerical result from Fig. 1(a) with the analytical result for σ_B from (4.9).[19] The latter is

[16] Although our free parameters Λ, G_D, and G_S coincide with the parameters used in [10], the numerical value of σ_0 is different from what is reported in [10]. The reason for this difference is apparently in the choice of the cutoff function. Whereas we use smooth cutoff function (5.2), in [10] a sharp momentum cutoff is used to perform the momentum integrations numerically.

[17] In (3.24), the integrals proportional to $\tilde{e}B$ and including a summation over Landau levels n arises from charged quarks with charges $\tilde{q} = \pm\frac{1}{2}, +1$.

[18] We have also checked our results for $A = 0.001\Lambda$ (quasisharp cutoff), where instead of small oscillations, small discontinuities appear in the regime $\tilde{e}B \lesssim 0.4\ \mathrm{GeV}^2$.

[19] For our specific choice of G_S and Λ from (5.1), the dimensionless coupling $0 < g_s < 1$. On the other hand, since no mixed phase is assumed here, σ_B from (4.9) in the regime $\mu < \sigma_B$ is the only relevant mass gap that can be compared with σ_B arising from our numerical calculation.

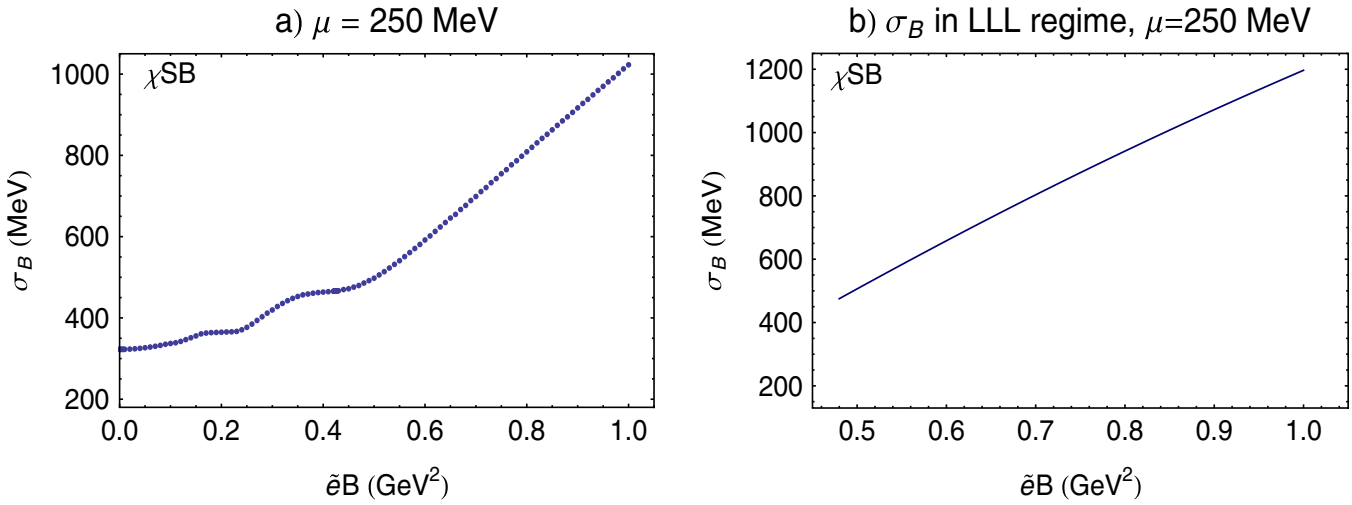

FIG. 1 (color online). (a) The dependence of σ_B on $\tilde{e}B$ in the χSB phase for $\mu = 250$ MeV; (b) The analytical result of σ_B in the regime of LLL dominance from (4.9) is plotted for $\tilde{e}B \in \{0.45, 1\}$ GeV^2 and $\mu = 250$ MeV.

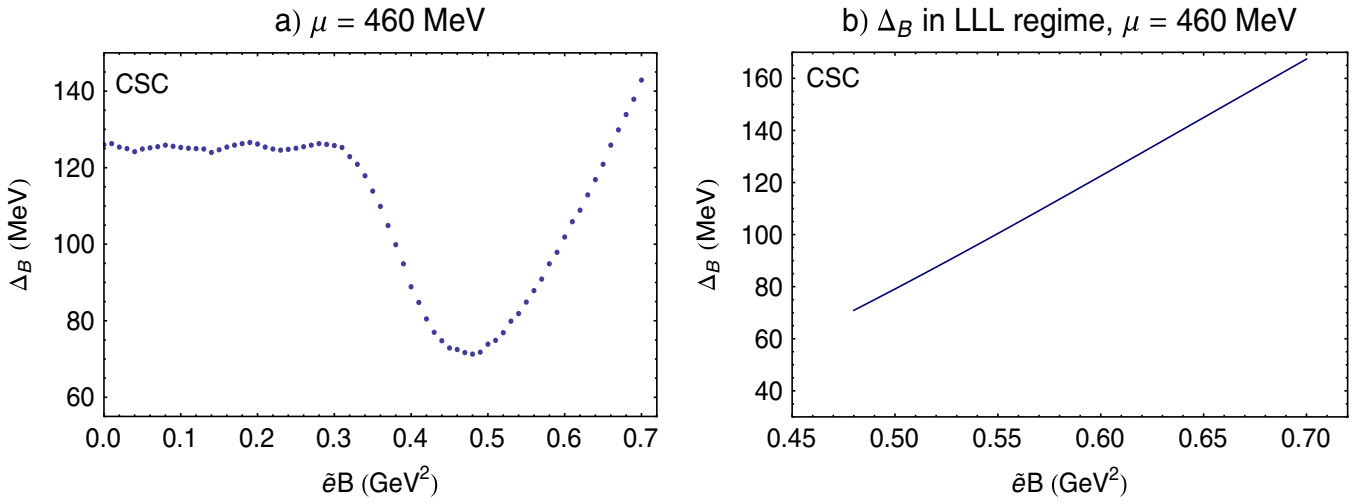

FIG. 2 (color online). (a) The dependence of Δ_B on $\tilde{e}B$ in the CSC phase for $\mu = 460$ MeV. (b) The analytical result of Δ_B in the regime of LLL dominance from (4.33) is plotted for $\tilde{e}B \in \{0.47, 1\}$ GeV^2.

plotted in Fig. 1(b) for the same interval of the magnetic field, i.e. $\tilde{e}B \in \{0.45, 1\}$ GeV^2. Similarly, in Fig. 2(a), the CSC mass gap Δ_B is plotted as a function of $\tilde{e}B$ for $\mu = 460$ MeV. Same small vAdH oscillations appear for small $\tilde{e}B \lesssim 0.47$ GeV^2. They are also observed in [22,23] for the diquark in the CFL superconducting phase. Small oscillations in Fig. 2(a), end up in a linear regime, that starts, as in the previous case, at $\tilde{e}B \gtrsim 0.47$ GeV^2. The qualitative behavior of Δ_B in this regime can be compared with the analytical result (4.33), that arises in the LLL approximation [Fig. 2(b)].

In Fig. 3, the dependence of the color chemical potential μ_8 on $\tilde{e}B$ is plotted for $\mu = 460$ MeV in the CSC phase. The vAdH oscillations in Fig. 3 are similar to the oscillations of μ_8 in the regime of small magnetic fields that are observed in [22] in the superconducting CFL model.

In summary, comparing the above numerical results with our analytical results from Sec. IV A and IV B for nonzero magnetic field, it turns out that there exists a threshold magnetic field $(\tilde{e}B)_t \simeq 0.45$–$0.50$ GeV^2, where the qualitative behavior of our numerical results coincides with the qualitative behavior of the analytical results for χSB and CSC mass gaps σ_B and Δ_B.[20] This regime, for which the LLL approximation seems to be reliable, will be denoted from now on by "the linear regime."[21]

[20]Note that the similarity in the numerical and analytical results for $\tilde{e}B > (\tilde{e}B)_t$ is only qualitative. This is because of various approximations that are carried out to determine the analytical results [see Sec. IV for more details].

[21]Note that in Figs. 2 and 3, the threshold magnetic field satisfies the requirement of LLL approximation $(\tilde{e}B)_t \gg \mu^2$.

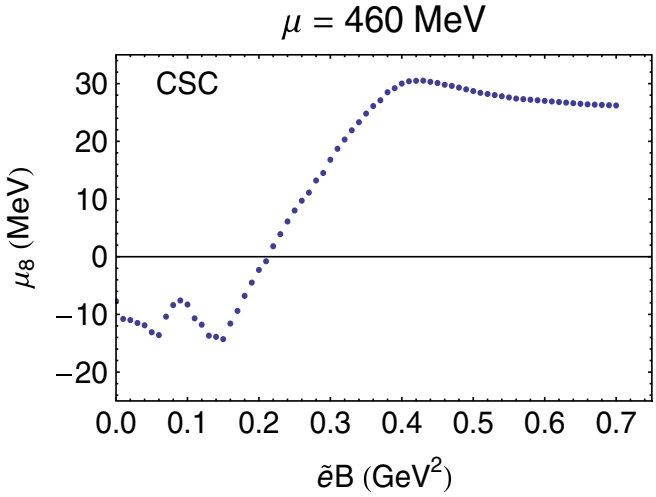

FIG. 3 (color online). The dependence of μ_8 on $\tilde{e}B$ in the CSC phase for $\mu = 460$ MeV. The vAdH oscillations are similar to the oscillations that are observed in [22] in the superconducting CFL model.

Using the above data, the magnetization of the 2SC superconducting medium can be studied as a function of $\tilde{e}B$ and for fixed chemical potential μ. Figure 4 shows the dependence of the product of the magnetization $\mathbf{M} = M\mathbf{e}_3$ with $M \equiv -\frac{\partial\Omega_{\text{eff}}^{(1)}}{\partial B}$ and the rotated magnetic field $\tilde{\mathbf{B}} = B\mathbf{e}_3$ as a function of $\tilde{e}B$ for two different chemical potential $\mu = 250$ MeV in the χSB regime and $\mu = 460$ MeV in the CSC regime [Figs. 4(a) and 4(b)]. Here $\Omega_{\text{eff}}^{(1)}$ is the one-loop part of the effective potential (3.24). For simplicity, we will use the definition $\mathbf{M}\cdot\tilde{\mathbf{B}} \equiv -\tilde{e}B\frac{\partial\Omega_{\text{eff}}^{(1)}}{\partial\tilde{e}B}$. Equivalently, one can define the magnetization by introducing the Gibbs free energy density $\mathcal{G}$ in the presence of a constant magnetic field B

$$\mathcal{G}(\sigma, \Delta; B, \mu) = \frac{B^2}{2} + \Omega_{\text{eff}}^{(1)}(\sigma, \Delta; B, \mu) - HB, \quad (5.3)$$

where H is the external magnetic field [23]. Whereas in vacuum $H = B$, in a medium with finite magnetization density, the external magnetic field H is different from the induced magnetic field B. Minimizing $\mathcal{G}$ with respect to B and evaluating the result at the minimum of the potential, we get the well-known relation $\mathbf{M} = \mathbf{B} - \mathbf{H}$, where $\mathbf{M}$ is the magnetization. Note that the minimum of the potential in the χSB phase is given by ($\sigma_B \neq 0$, $\Delta_B = \mu_8 = 0$) and in the CSC phase by ($\sigma_B = 0$, $\Delta_B \neq 0$, $\mu_8 \neq 0$). The magnetization of the superconducting CFL phase is studied as a function of eB/μ^2 for $\mu = 500$ MeV in [23], where the same vAdH oscillations as appears in Fig. 4 are observed.

In what follows, we will first study the μ-dependence of σ_B and Δ_B. We then present the phase diagram μ_c-$\tilde{e}B$ of the 2SC quark matter at zero temperature. Let us start with the case of zero magnetic field. In Fig. 5, the μ-dependence of σ_0 in the χSB phase, as well as Δ_0 and μ_8 in the CSC phase are plotted for zero magnetic field. For our specific choice of free parameters Λ, G_S and G_D, $\sigma_0 = 323.8$ MeV for $\mu \leq \mu_c$. Here, the critical chemical potential $\mu_c = 325$ MeV and the value of Δ_0 for $\mu \simeq \mu_c$ is $\Delta_0 = 78.0$ MeV. Our results coincides qualitatively with the numerical results presented in [6] (see also [40] for a recent investigation of Cooper-pairing in NJL-type models).[22]

We can compare the μ-dependence of Δ_0^2 arising from our numerical calculation with the relation (4.39) arising from our analytical results for vanishing magnetic field. To do this we have fitted our numerical data with a function

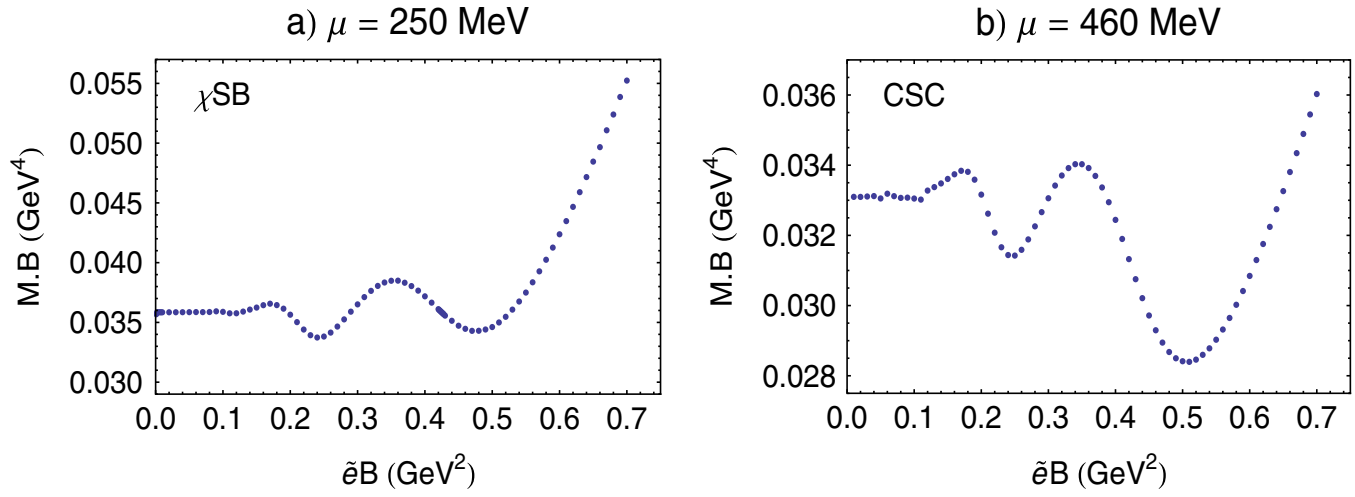

FIG. 4 (color online). The dependence of the product $\mathbf{M}\cdot\tilde{\mathbf{B}}$ on the magnetic field of fixed chemical potential (a) $\mu = 250$ MeV in the χSB phase and (b) $\mu = 460$ MeV in the CSC phase. The linear regime in both phases starts at $\tilde{e}B \simeq 0.45$–0.50 GeV^2.

[22]In [6], the quark mass $m_0 \neq 0$ and therefore a mixed phase appears for $\mu \geq 340$ MeV.

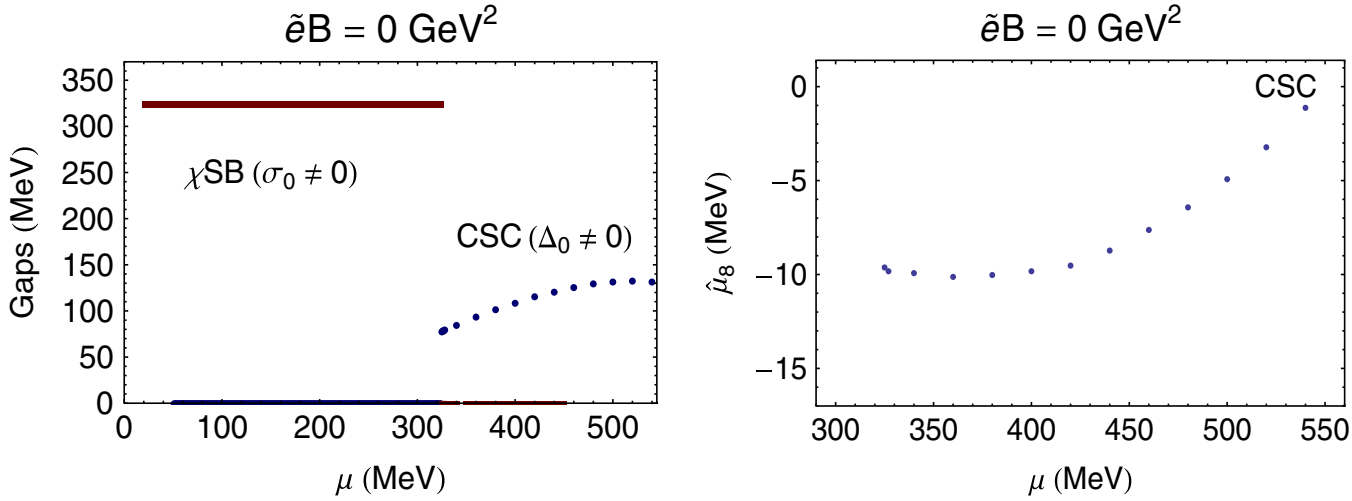

FIG. 5 (color online). The μ-dependence of σ_0 in the χSB phase, and Δ_0 in the CSC phase for $\tilde{e}B = 0$ (left panel). The μ-dependence of $\hat{\mu}_8$ for $\tilde{e}B = 0$ (right panel).

$$\Delta_0^2(\mu) = (a - b\mu^2)\exp\left(-\frac{c}{\mu^2}\right), \tag{5.4}$$

similar to (4.39). Here, a, b, and c are free parameters. The numerical values of these parameters arising from our fit are in good agreement with the expected analytical values arising from (4.39) (see Fig. 6 and Table II). This can be quantified by defining

$$\eta \equiv \left|\frac{\text{Analytical value} - \text{Numerical value}}{(\text{Analytical value} + \text{Numerical value})/2}\right|, \tag{5.5}$$

as a measure for the variation of the numerical value with respect to the average of analytical and numerical values. In Table II, η_a, η_b and η_c are less than 50%. Note that the difference between the analytical and numerical values of a, b and c lies on the approximations that are made to determine analytically Δ_0^2 in (4.39).

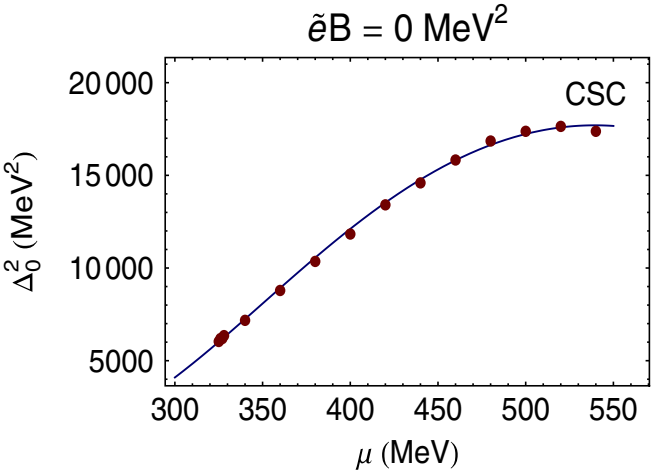

FIG. 6 (color online). The dots are the numerical values of Δ_0^2. The solid line is the corresponding fit of $\Delta_0^2(\mu)$ from (5.4). The fit parameters a, b, and c are listed in Table II. The regression parameter R^2, as a measure of reliability of the numerical fit, is in this case $R^2 = 0.999\,852$.

Let us now concentrate on the case of nonvanishing magnetic field. In Table III, we have summarized our numerical results for critical chemical potential μ_c, the mass gap σ_B for $\mu \leq \mu_c$ and the 2SC gap Δ_B at $\mu \simeq \mu_c$. The critical chemical potential μ_c and the χSB mass gaps $\sigma_B(\mu \leq \mu_c)$ increase by increasing the external magnetic field. In the vicinity of the phase transition from χSB to CSC phase, the CSC mass gap $\Delta_B(\mu \simeq \mu_c)$ also increases by increasing the magnetic field.

The μ-dependence of σ_B and Δ_B are presented also in Fig. 7. There is a first order phase transition from the χSB to the CSC phase [see also Fig. 9 for more detail on the phase structure in μ_c-$\tilde{e}B$ plane]. Because of our specific choice $m_0 = 0$ and $G_D < G_S$, no mixed broken phase appears at $\mu > \mu_c$ [10], and the χSB mass gap $\sigma_B(\mu)$ is constant for $\mu \leq \mu_c$. For small value of $\tilde{e}B$, the CSC mass gap $\Delta_B(\mu, \tilde{e}B)$, is increasing with μ. The magnetic field

TABLE II. Numerical fit data for $\Delta_0^2(\mu)$ from (5.4). The numerical values of the parameters arising from our fit are in good agreement with the expected analytical values arising from (4.39) [see η_a, η_b, and η_c with η defined in (5.5)].

	Analytical parameters			Numerical fit parameters			η in %		
$\tilde{e}B$ (GeV^2)	a (MeV^2)	b	c (MeV^2)	a (MeV^2)	b	c (MeV^2)	η_a	η_b	η_c
0	8.49×10^4	0.19	2.29×10^5	7.84×10^4	0.13	2.52×10^5	8	38	10

TABLE III. Numerical results for critical chemical potential μ_c, the mass gap σ_B for $\mu \leq \mu_c$ and the 2SC gap Δ_B at $\mu \simeq \mu_c$.

$\tilde{e}B$ in GeV^2	μ_c in MeV	$\sigma_B(\mu \leq \mu_c)$ in MeV	$\Delta_B(\mu \simeq \mu_c)$ in MeV
0.002	316.0	312.0	70.0
0.005	287.0	311.0	61.0
0.01	324.2	322.4	78.0
0.04	322.3	326.4	77.6
0.05	321.9	327.8	77.9
0.10	311.3	338.4	76.9
0.20	296.0	366.0	50.8
0.30	315.0	420.7	73.2
0.40	329.0	464.8	80.4
0.46	329.6	477.0	82.6
0.48	334.0	487.0	85.7
0.50	340.8	499.0	88.8
0.60	392.4	593.0	116.9
0.70	450.7	700.0	147.7

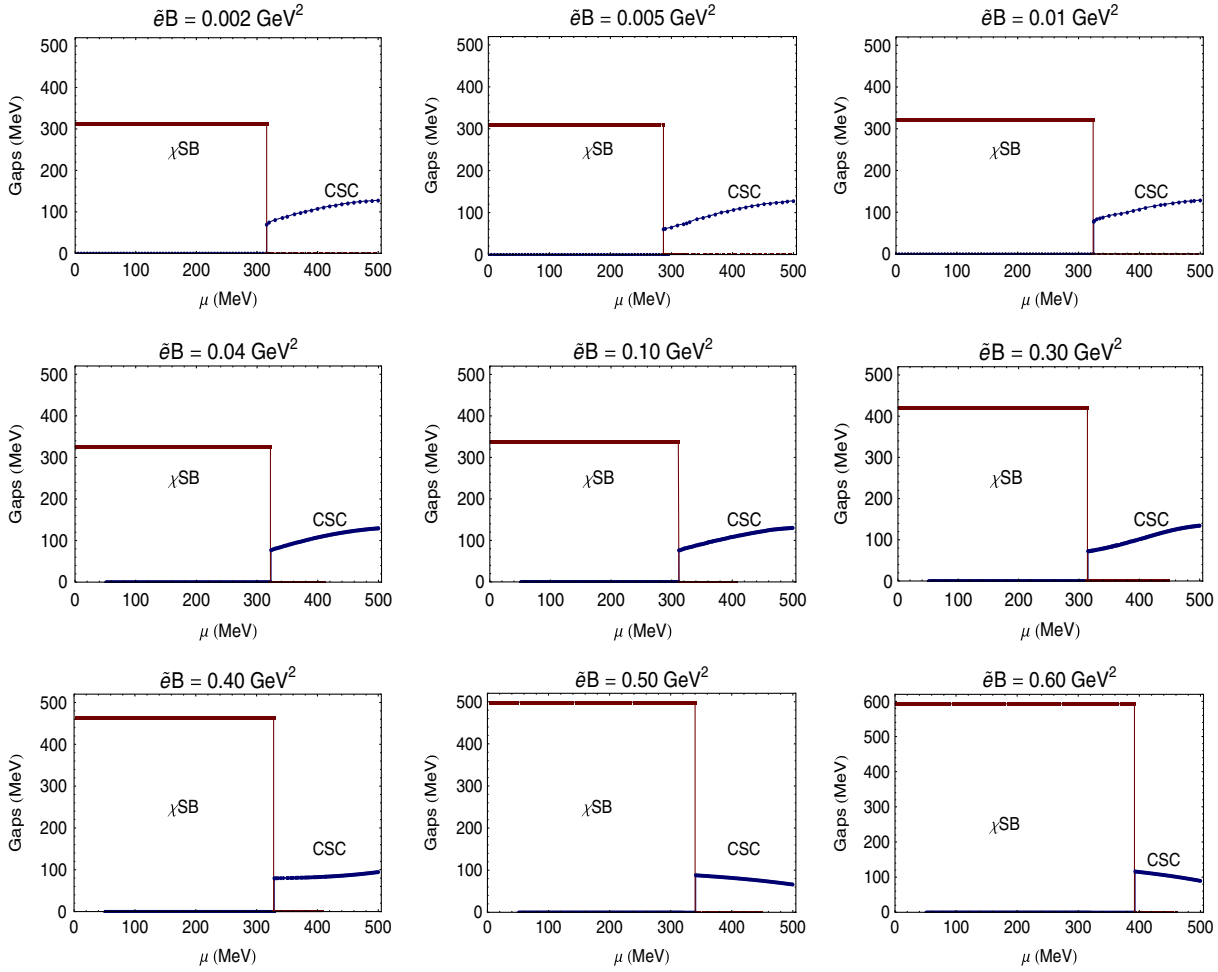

FIG. 7 (color online). The μ-dependence of σ_B in the χSB phase (red lines), and Δ_B in the CSC phase (blue lines) for different values of $\tilde{e}B$. The χSB mass gap $\sigma_B(\mu, \tilde{e}B)$ is constant in $\mu \leq \mu_c$ and increases for increasing $\tilde{e}B$. The critical chemical potential μ_c increases for increasing $\tilde{e}B$. For our specific choice of parameters ($m_0 = 0$, $G_D < G_S$) no mixed phase appears. The CSC mass gap Δ_B exists therefore only at $\mu > \mu_c$. The slopes of the curves appearing at $\mu > \mu_c$ are decreasing for increasing $\tilde{e}B$. The first order nature of the phase transition between χSB and CSC phases is visible. The dependence of the χSB and CSC gaps for vanishing magnetic field is also considered here to have a comparison with the μ-dependence of the gaps for nonvanishing $\tilde{e}B$.

TABLE IV. Numerical fit data for Δ_B^2 as a function of μ from (5.6). In the linear regime, i.e. for $\tilde{e}B \gtrsim 0.45$ GeV^2, the numerical values of the parameters arising from our fit are in good agreement with the expected analytical values of the parameters from (4.33) [see η_a and η_b with η defined in (5.5)].

	Analytical parameters		Numerical fit parameters		η in %	
$\tilde{e}B$ (GeV^2)	a (MeV^2)	b	a (MeV^2)	b	η_a	η_b
0.04	5.27×10^{-24}	1.32×10^{-28}	-1.06×10^{3}	-0.077	200	200
0.10	1.62×10^{-6}	1.62×10^{-11}	-8.37×10^{2}	-0.077	200	200
0.30	1.91×10^{2}	6.37×10^{-4}	-4.53×10^{3}	-0.094	218	201
0.40	2.27×10^{3}	0.006	$+4.17 \times 10^{3}$	-0.018	59	400
0.44	4.53×10^{3}	0.010	$+7.38 \times 10^{3}$	$+0.008$	48	22
0.46	6.14×10^{3}	0.013	$+8.47 \times 10^{3}$	$+0.015$	32	14
0.50	1.05×10^{4}	0.021	$+1.09 \times 10^{4}$	$+0.025$	4	17
0.60	3.03×10^{4}	0.050	$+2.26 \times 10^{4}$	$+0.058$	29	15

enhances the chiral symmetry breaking. This is known as the phenomenon of magnetic catalysis [28], which is also observed in [32]. In the linear regime, i.e. for $\tilde{e}B \gtrsim 0.45$ GeV^2, Δ_B is decreasing with μ. To study the linear regime in detail, we have fitted our numerical data for Δ_B as a function of μ and fixed $\tilde{e}B$, with a function similar to (4.33)

$$\Delta_B^2 = (a - b\mu^2), \tag{5.6}$$

where a and b are free parameters, that depend on $\tilde{e}B$. In Table IV, we have compared the expected analytical results for the parameters a and b, with the corresponding results from fitting our numerical data with (5.6) for different $\tilde{e}B$. For $\tilde{e}B \gtrsim 0.44$ GeV^2, η_a and η_b are less than 50%.

In Fig. 8, the μ-dependence of the color chemical potential μ_8 for different $\tilde{e}B$ is demonstrated. As in the previous cases, we expect that, in the linear regime $\tilde{e}B \gtrsim 0.45$ GeV^2, the μ dependence of μ_8 is given by a function similar to (4.30), that arises analytically in the LLL approximation. We, therefore, define a function

$$\mu_8 = \frac{\mu^3}{a + b\mu^2}, \tag{5.7}$$

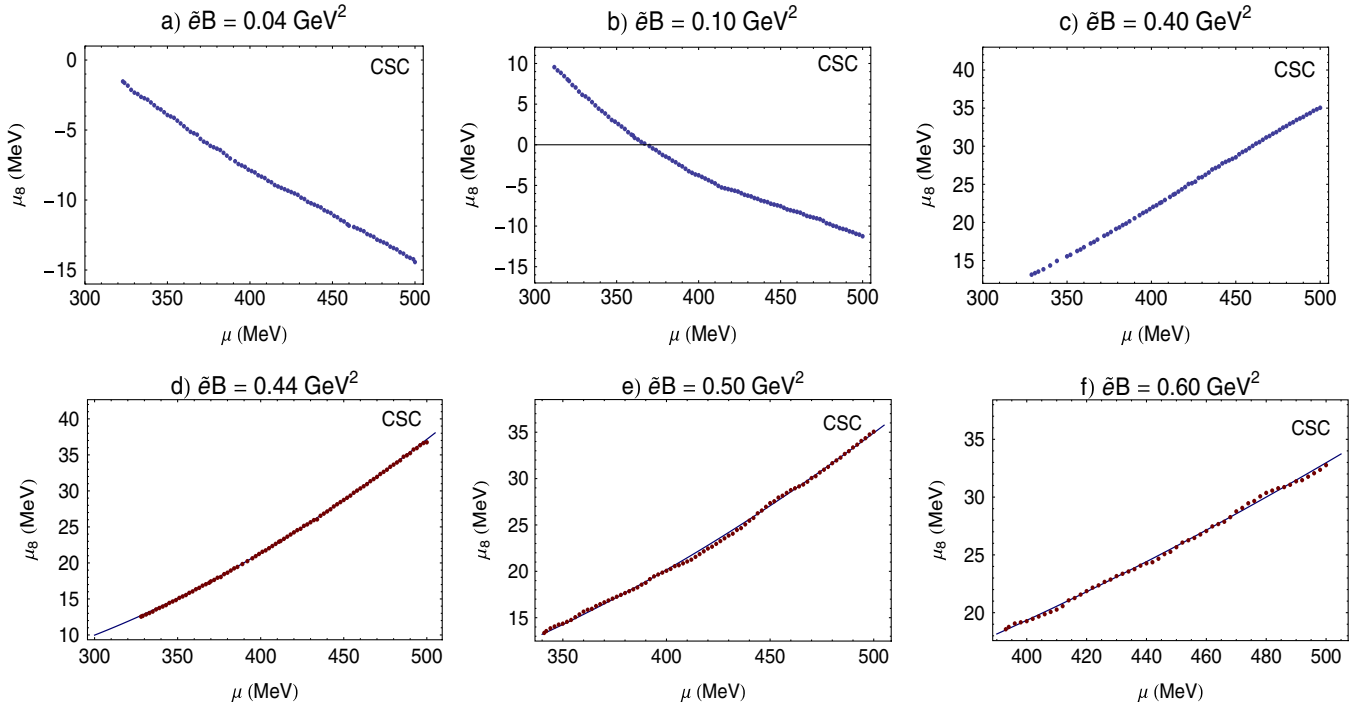

FIG. 8 (color online). The μ-dependence of the color chemical potential μ_8 as a function. The numerical data for μ_8 are fitted in Figs 8d–8f by (5.7). In the linear regime, the fitted curves [solid (blue) lines in 8d–8f] are in good agreement with our numerical data. For $\tilde{e}B = 0.44$, 0.5 GeV^2, and 0.6 GeV^2, the regression parameter R^2, as a measure of reliability of numerical fits are $R^2 = 0.999\,991$, 0.999 924, 0.999 952, respectively.

TABLE V. Numerical fit data for μ_8 as a function of μ from (5.7). In the linear regime, i.e. for $\tilde{e}B \gtrsim 0.40$ GeV^2, the numerical values of the parameters arising from our fit are in good agreement with the expected analytical values of the parameters from (4.30) [see η_a and η_b with η defined in (5.5)].

	Analytical parameters		Numerical fit parameters		η in %	
$\tilde{e}B$ (GeV^2)	a (MeV^2)	b	a (MeV^2)	b	η_a	η_b
0.04	1.80×10^5	6	-1.01×10^7	+7.53	207	23
0.10	4.50×10^5	6	-4.93×10^7	+161.14	204	186
0.30	1.35×10^6	6	$+3.04 \times 10^6$	+13.04	77	74
0.40	1.80×10^6	6	$+1.93 \times 10^6$	+6.27	7	4
0.44	1.98×10^6	6	$+2.34 \times 10^6$	+4.11	17	37
0.46	2.07×10^6	6	$+2.43 \times 10^6$	+3.89	16	43
0.50	2.25×10^6	6	$+2.46 \times 10^6$	+4.49	9	29
0.60	2.70×10^6	6	$+2.45 \times 10^6$	+5.35	10	11

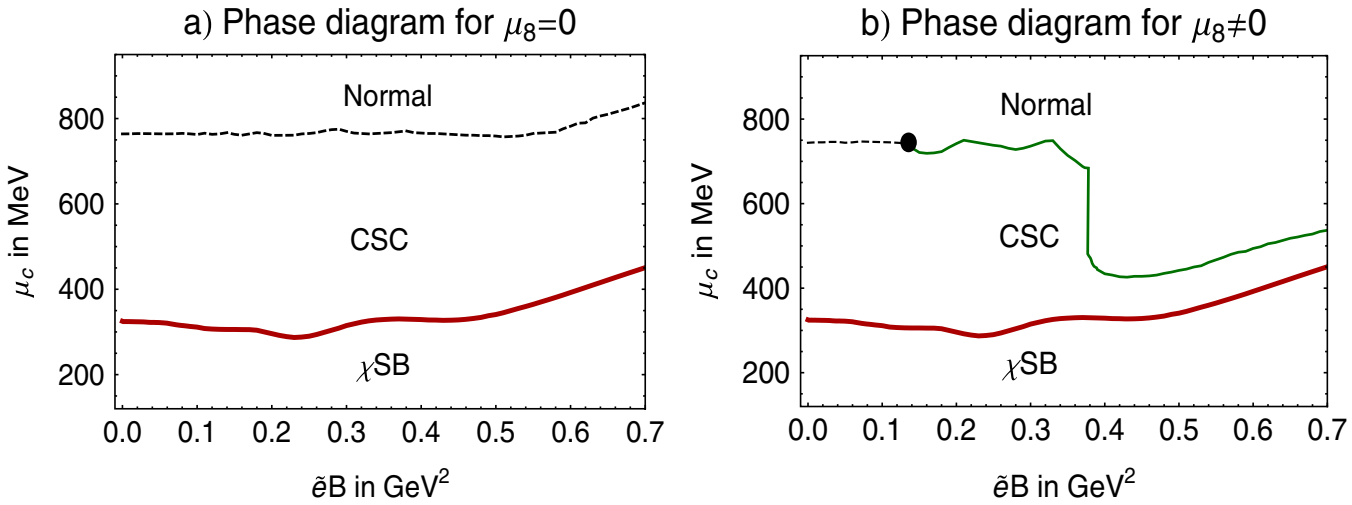

FIG. 9 (color online). The phase diagram of 2SC model is plotted in a μ_c-$\tilde{e}B$ plane for (a) $\mu_8 = 0$ and (b) $\mu_8 \neq 0$. The solid thick (red) lines in (a) and (b) indicate first order phase transitions between the χSB and the CSC phase. The dashed (black) lines in (a) and (b) are second order critical lines between the CSC and the normal phase. As it is shown in (b), for $\mu_8 \neq 0$ and at $\mu_c \simeq 755$ MeV and $\tilde{e}B \simeq 0.13$ GeV^2, the second order phase transition goes over into a first order phase transition between the CSC and the normal phase [solid thin (green) line]. At $\tilde{e}B \simeq 0.4$ GeV^2, μ_c suddenly decreases and increases once again by increasing the external magnetic fields in the CSC regime.

with arbitrary, $\tilde{e}B$-dependent parameters a and b. In Table V, we have compared the data that arise numerically by fitting the numerical values of μ_8 with (5.7) for different $\tilde{e}B$. As in the previous case, the difference between the numerical fit data and the expected analytical values of a and b arising from (4.30) minimizes in the linear regime for $\tilde{e}B \gtrsim 0.40$ GeV^2 (η_a and η_b in Table V are less than 50%.).

Finally, we will present the phase structure of the model in a μ_c-$\tilde{e}B$ plane in Fig. 9. In particular, we are interested on the effect of the color chemical potential μ_8 on the phase structure of the model. In Fig. 9(a) [Fig. 9(b)] the phase structure for $\mu_8 = 0$ ($\mu_8 \neq 0$) is plotted. Because of our specific choice of parameters, we expect χSB and CSC phase without mixing. A normal phase can also exist, where the mass gaps σ_B and Δ_B corresponding to χSB and CSC phases vanish identically.[23] To check this, we consider the gap equations and the color neutrality condition (4.1). We have looked for the global minima of the

[23]As it is known from [5], in the regime of large chemical potential, $\mu \gtrsim 500$ MeV, the 2SC phase goes over into the three-flavor CFL phase. In the present two-flavor model, we only assume that a normal phase may exist, and, if so a phase transition will occur from the color superconducting 2SC phase into this normal phase (see Fig. 9). Hence, the present results concerning the transition from CSC to the normal phase are only of theoretical nature. To include the CFL phase, we have to extend the model to three-flavor superconductivity including up, down, and strange quarks. This is indeed beyond the scope of the present paper and is planned for future publications.

system in two different regimes: $\mu_c \simeq 350$–450 MeV and $\mu_c \simeq 750$–800 MeV. As it turns out, in the first regime corresponding to $\mu_c \simeq 350$–450 MeV, the minima of Ω_{eff} from (3.24) are given by $(\sigma_B \neq 0,\ \Delta_B = 0,\ \mu_8 = 0)$ for $\mu < \mu_c$ as well as $(\sigma_B = 0, \Delta_B \neq 0, \mu_8 \neq 0)$ for $\mu > \mu_c$. In the second regime corresponding to $\mu_c \simeq 750$–800 MeV, however, the global minima are $(\sigma_B = 0, \Delta_B \neq 0, \mu_8 \neq 0)$ for $\mu < \mu_c$, as well as $(\sigma_B = 0, \Delta_B = 0, \mu_8 = 0)$ for $\mu > \mu_c$. We conclude therefore that a phase transition from χSB to CSC phase occurs in the first regime at $\mu_c \simeq 350$–450 MeV, and a phase transition from CSC to the normal phase occurs in the second regime $\mu_c \simeq 750$–800 MeV. In the following, we denote the value of Ω_{eff} at the global minima by $\Omega_{\chi\text{SB}} \equiv \Omega_{\text{eff}}(\sigma_B, 0, 0; \mu, \tilde{e}B)$, $\Omega_{\text{CSC}} \equiv \Omega_{\text{eff}}(0, \Delta_B, \mu_8; \mu, \tilde{e}B)$, and $\Omega_{\text{Normal}} \equiv \Omega_{\text{eff}}(0, 0, 0; \mu, \tilde{e}B)$ corresponding to the χSB, CSC and the normal phase, respectively. For different values of $(\mu, \tilde{e}B)$, the χSB phase is defined by $\Omega_{\chi\text{SB}} \leq \Omega_{\text{CSC}}$ and the CSC phase by $\Omega_{\text{CSC}} \leq \Omega_{\chi\text{SB}}$. Moreover, the exact value of μ_c for the first order phase transition from χSB to the CSC phase [the thick (red) solid line in Fig. 9(a) and 9(b)] and from the CSC phase to the χSB phase [thin (green) solid line in Fig. 9(b)] are then defined by $\Omega_{\chi\text{SB}} = \Omega_{\text{CSC}}$ and $\Omega_{\text{CSC}} = \Omega_{\text{Normal}}$, respectively [34]. As for the second order phase transition between the CSC and the normal phase, an analysis similar to [8] is performed. In Fig. 9(a), the phase diagram of the 2SC model in a μ_c-$\tilde{e}B$ plane is plotted for vanishing μ_8. A first order phase transition occurs between the χSB and the CSC phase in the regime $\mu_c \simeq 350$–450 MeV (solid red line). This confirms the results by [26], where a first order phase transition is observed for fixed value of $\tilde{e}B = 0.05$ GeV^2, and various G_D/G_S. The transition from the CSC into the normal phase is of second order and occurs in the regime $\mu_c \simeq 750$–800 MeV (dashed black line). According to the phase diagram for nonvanishing μ_8 in Fig. 9(b), however, whereas the transition from the χSB to CSC phase is still of first order (solid red line), the second order phase transition for small values of $\tilde{e}B$ (dashed black line) goes over into a first order phase transition at $\mu_c \simeq 755$ MeV and $\tilde{e}B \simeq 0.13$ GeV^2 (solid green line). Moreover, at $\tilde{e}B \simeq 0.4$ GeV^2, μ_c suddenly decreases and increases once again by increasing the external magnetic fields in the CSC regime. The CSC regime is nevertheless suppressed in the linear regime $\tilde{e}B \gtrsim 0.45$ GeV^2 by the external magnetic field [see Fig. 9(b)].

VI. CONCLUDING REMARKS

In this paper, we have studied the effect of constant magnetic fields on the formation of bound states in the chiral as well as the color symmetry breaking phase. In the first part of the paper, after introducing a two-flavor NJL type model including meson and diquark condensates, we have computed the one-loop effective action and the thermodynamic potential of the theory at zero temperature and finite density. Neglecting the quark mass m_0 and choosing the diquark-to-chiral coupling ratio $G_D/G_S < 1$ [10], we can consider the χSB and CSC phases separately. The χSB and CSC mass gaps σ_B and Δ_B as well as the color chemical potential μ_8 are determined analytically in the limit of very strong magnetic fields. In this limit, the dynamics of the system is dominated by the lowest Landau level and therefore the effect of all higher Landau levels is negligible. According to [28], in this limit, as a result of dimensional reduction from D to $D-2$ dimensions, the formation of bound states and consequently a dynamical symmetry breaking will be possible even for weak interactions between two fermions. This is the phenomenon of magnetic catalysis, discussed widely in the literature in the past few years [29–31]. Denoting the dimensionless coupling constants in the χSB and CSC phases by $g_s \sim G_S\Lambda^2$ and $g_d \sim G_D\Lambda^2$, we have determined the mass gaps for different regimes of g_s and g_d. Here, Λ is certain momentum cutoff. In [6], the χSB and CSC mass gaps of a similar 2SC model were determined numerically for vanishing magnetic field. Introducing a large momentum cutoff Λ and performing appropriate approximations, we have determined analytically the mass gaps σ_0 and Δ_0 as well as μ_8 corresponding to χSB and CSC phases for zero magnetic field too.

In the second part of the paper, a detailed numerical analysis is performed to explore the effect of any arbitrary magnetic field on the mass gaps σ and Δ and the color chemical potential μ_8. First, the dependence of σ and Δ on various $\tilde{e}B \in [0, 1]$ GeV^2 is plotted for fixed $\mu = 250$ MeV and $\mu = 460$ MeV in the χSB and CSC phases, respectively. For small values of $\tilde{e}B$, we observe small van Alfven-de Haas oscillations, that appear, according to [22,23] also in the CFL phase for $\mu = 500$ MeV. The same oscillations appear also in the magnetization M for the same fixed value of chemical potentials. At $\tilde{e}B \simeq 0.4$–0.5 GeV^2, the oscillations end up in a linear regime, where we believe that the dynamics of the system is described exclusively by the LLL. This can be checked by comparing qualitatively the numerical dependence of σ_B and Δ_B for $\tilde{e}B \geq 0.45$ GeV^2 and fixed μ. The μ-dependence of σ and Δ are then considered for various $\tilde{e}B$. Our numerical results for vanishing magnetic field coincide with the numerical results presented in [6]. The μ-dependence of σ_B and Δ_B as well as μ_8 are then considered for various finite $\tilde{e}B$. The numerical results in the linear regime, i.e. for $\tilde{e}B \gtrsim 0.45$ GeV^2 are comparable with our before mentioned analytical results in the limit of large $\tilde{e}B$. This is shown using appropriate numerical fits. The phase structure of the χSB and CSC phases in a μ_c-$\tilde{e}B$ plane is also presented. We are, in particular, interested on the effect of the color chemical potential μ_8 on the phase diagram of the model. For both $\mu_8 = 0$ as well as $\mu_8 \neq 0$, the transition from the χSB phase into the CSC phase is of first order, and occurs in the regime $\mu_c \simeq 350$–450 MeV

and for $\tilde{e}B \in [0, 0.7]$ GeV^2 [see Fig. 9(a)]. This confirms the result in [26], where a first-order phase transition is observed between the χSB and CSC phase for fixed $\tilde{e}B = 0.05$ GeV^2 and various G_D/G_S ratios. Assuming that the CSC phase goes over into a normal phase at $\mu > 500$ MeV,[24] it turns out that whereas for $\mu_8 = 0$, this transition is of second order, for nonvanishing μ_8, a second-order phase transition occurs first for small $\tilde{e}B$. It goes then over into a first order phase transition at $\mu_c \simeq 755$ MeV and $\tilde{e}B \simeq 0.13$ GeV^2. At $\tilde{e}B \simeq 0.4$ GeV^2, μ_c suddenly decreases and increases once again by increasing the external magnetic fields. The CSC phase is nevertheless suppressed in the linear regime $\tilde{e}B \gtrsim 0.45$ GeV^2 by the external magnetic field [see Fig. 9(b)].

In the end, let us just emphasize that the study of color superconductivity in the presence of constant magnetic fields has not only astrophysical consequences in forming the structure of compact star cores, it may be also relevant for future heavy ion collision experiments. Recently in [17], the accessibility of the color superconducting 2SC phase in the heavy ion collisions is investigated. It is stated that for high enough collision energies the 2SC may be accessible in future collision experiments. On the other hand, there are various evidences of the creation of very strong magnetic fields in noncentral heavy ion collisions [15,16]. It would be interesting to perform similar analysis as in [17] considering the presence of constant magnetic fields. To do this, the effect of finite temperature on the phase diagram of the 2SC superconducting phase in the presence of constant magnetic fields also has to be considered. This will be reported in future publications [11].

[24]See footnote 23.

ACKNOWLEDGMENTS

Sh. F. thanks F. Farahpour for useful discussions on numerical results, and H. Hadipour for discussions on high T_c-superconductivity, N. S. thanks M. Bahmanabadi and S. Rahvar for discussions on the numerical fit data. Both authors thank F. Ardalan, H. Arfaei, A. E. Mosaffa for discussions and E. J. Ferrer for email correspondence.

[1] D. Bailin and A. Love, Nucl. Phys. **B205**, 119 (1982); M. G. Alford, K. Rajagopal, and F. Wilczek, Nucl. Phys. **B537**, 443 (1999); D. T. Son, Phys. Rev. D **59**, 094019 (1999); T. Schafer and F. Wilczek, Phys. Rev. D **60**, 114033 (1999); D. K. Hong, V. A. Miransky, I. A. Shovkovy, and L. C. R. Wijewardhana, Phys. Rev. D **61**, 056001 (2000); **62**, 059903(E) (2000); R. D. Pisarski and D. H. Rischke, Phys. Rev. D **61**, 051501 (2000).

[2] Y. Nambu and G. Jona-Lasinio, Phys. Rev. **122**, 345 (1961); **124**, 246 (1961).

[3] M. G. Alford, K. Rajagopal, and F. Wilczek, Phys. Lett. B **422**, 247 (1998); R. Rapp, T. Schafer, E. V. Shuryak, and M. Velkovsky, Phys. Rev. Lett. **81**, 53 (1998).

[4] M. G. Alford, Annu. Rev. Nucl. Part. Sci. **51**, 131 (2001); K. Rajagopal and F. Wilczek, arXiv:hep-ph/0011333; G. Nardulli, Riv. Nuovo Cimento Soc. Ital. Fis. **25N3**, 1 (2002).

[5] M. Buballa, Phys. Rep. **407**, 205 (2005); M. Huang, Int. J. Mod. Phys. E **14**, 675 (2005); I. A. Shovkovy, Found. Phys. **35**, 1309 (2005); M. G. Alford, A. Schmitt, K. Rajagopal, and T. Schafer, Rev. Mod. Phys. **80**, 1455 (2008).

[6] D. Ebert, K. G. Klimenko, and V. L. Yudichev, Phys. Rev. D **72**, 056007 (2005).

[7] M. Buballa and I. A. Shovkovy, Phys. Rev. D **72**, 097501 (2005).

[8] J. Berges and K. Rajagopal, Nucl. Phys. **B538**, 215 (1999).

[9] T. M. Schwarz, S. P. Klevansky, and G. Papp, Phys. Rev. C **60**, 055205 (1999); B. Vanderheyden and A. D. Jackson, Phys. Rev. D **62**, 094010 (2000).

[10] M. Huang, P. f. Zhuang, and W. q. Chao, Phys. Rev. D **67**, 065015 (2003).

[11] Sh. Fayyazbakhsh and N. Sadooghi (work in progress).

[12] C. Thompson and R. C. Duncan, Astrophys. J. **473**, 322 (1996).

[13] V. de la Incera, arXiv:1004.4931.

[14] D. E. Kharzeev, L. D. McLerran, and H. J. Warringa, Nucl. Phys. **A803**, 227 (2008); H. J. Warringa, J. Phys. G **35**, 104012 (2008).

[15] I. V. Selyuzhenkov (STAR Collaboration), Romanian reports in Physics **58**, 049 (2006).

[16] V. Skokov, A. Y. Illarionov, and V. Toneev, Int. J. Mod. Phys. A **24**, 5925 (2009).

[17] D. B. Blaschke, F. Sandin, V. V. Skokov, and S. Typel, Acta Phys. Pol. B **3**, 741 (2010).

[18] M. G. Alford, J. Berges, and K. Rajagopal, Nucl. Phys. **B571**, 269 (2000).

[19] E. V. Gorbar, Phys. Rev. D **62**, 014007 (2000).

[20] E. J. Ferrer, V. de la Incera, and C. Manuel, Nucl. Phys. **B747**, 88 (2006); E. J. Ferrer and V. de la Incera, Phys. Rev. D **76**, 114012 (2007).

[21] E. J. Ferrer, V. de la Incera, and C. Manuel, Phys. Rev. Lett. **95**, 152002 (2005); E. J. Ferrer and V. de la Incera, Phys. Rev. D **76**, 045011 (2007).

[22] K. Fukushima and H. J. Warringa, Phys. Rev. Lett. **100**, 032007 (2008).

[23] J. L. Noronha and I. A. Shovkovy, Phys. Rev. D **76**, 105030 (2007).

[24] D. Ebert and A. S. Vshivtsev, arXiv:hep-ph/9806421.

[25] M. G. Alford and A. Sedrakian, J. Phys. G **37**, 075202

(2010); X. G. Huang, M. Huang, D. H. Rischke, and A. Sedrakian, Phys. Rev. D **81**, 045015 (2010).
[26] T. Mandal, P. Jaikumar, and S. Digal, arXiv:0912.1413.
[27] K. G. Klimenko, Z. Phys. C **54**, 323 (1992); V. P. Gusynin, V. A. Miransky, and I. A. Shovkovy, Phys. Rev. Lett. **73**, 3499 (1994); **76**, 1005(E) (1996).
[28] V. P. Gusynin, V. A. Miransky, and I. A. Shovkovy, Nucl. Phys. **B462**, 249 (1996); D. S. Lee, C. N. Leung, and Y. J. Ng, Phys. Rev. D **55**, 6504 (1997).
[29] E. Elizalde, E. J. Ferrer, and V. de la Incera, Phys. Rev. D **70**, 043012 (2004); E. J. Ferrer and V. de la Incera, Int. J. Mod. Phys. A **19**, 5385 (2004).
[30] K. Farakos and N. E. Mavromatos, Phys. Rev. B **57**, 3017 (1998); V. C. Zhukovsky, K. G. Klimenko, V. V. Khudyakov, and D. Ebert, Pis'ma Zh. Eksp. Teor. Fiz. **73**, 137 (2001) [JETP Lett. **73**, 121 (2001)]; E. J. Ferrer, V. P. Gusynin, and V. de la Incera, Mod. Phys. Lett. B **16**, 107 (2002); E. V. Gorbar, V. P. Gusynin, V. A. Miransky, and I. A. Shovkovy, Phys. Rev. B **78**, 085437 (2008).
[31] K. G. Klimenko and V. C. Zhukovsky, Phys. Lett. B **665**, 352 (2008); E. Rojas, A. Ayala, A. Bashir, and A. Raya, Phys. Rev. D **77**, 093004 (2008); N. Sadooghi and K. S. Anaraki, Phys. Rev. D **78**, 125019 (2008); E. J. Ferrer and V. de la Incera, Phys. Rev. Lett. **102**, 050402 (2009); A. Ayala, A. Bashir, A. Raya, and A. Sanchez, Phys. Rev. D **80**, 036005 (2009); E. J. Ferrer and V. de la Incera, Nucl. Phys. **B824**, 217 (2010); N. Sadooghi, arXiv:0905.2097; A. Ayala, A. Bashir, A. Raya, and A. Sanchez, J. Phys. G **37**, 015001 (2010).
[32] T. Inagaki, D. Kimura, and T. Murata, Prog. Theor. Phys. **111**, 371 (2004).
[33] D. P. Menezes, M. Benghi Pinto, S. S. Avancini, A. Perez Martinez, and C. Providencia, Phys. Rev. C **79**, 035807 (2009).
[34] S. Kanemura, H. T. Sato, and H. Tochimura, Nucl. Phys. **B517**, 567 (1998).
[35] V. I. Ritus, Ann. Phys. (N.Y.) **69**, 555 (1972); Zh. Eksp. Teor. Fiz. **75**, 1560 (1978) [Sov. Phys. JETP **48**, 788 (1978)].
[36] E. Elizalde, E. J. Ferrer, and V. de la Incera, Ann. Phys. (N.Y.) **295**, 33 (2002).
[37] K. Fukushima, D. E. Kharzeev, and H. J. Warringa, Nucl. Phys. **A836**, 311 (2010).
[38] S. B. Ruester, arXiv:nucl-th/0612090.
[39] R. M. Coreless, G. H. Gonnet, D. E. G. Hare, D. J. Jeffrey, and D. E. Knuth, Adv. Comput. Math. **5**, 329 (1996).
[40] D. Ebert and K. G. Klimenko, arXiv:1005.0699.
[41] L. Campanelli and M. Ruggieri, Phys. Rev. D **80**, 034014 (2009).